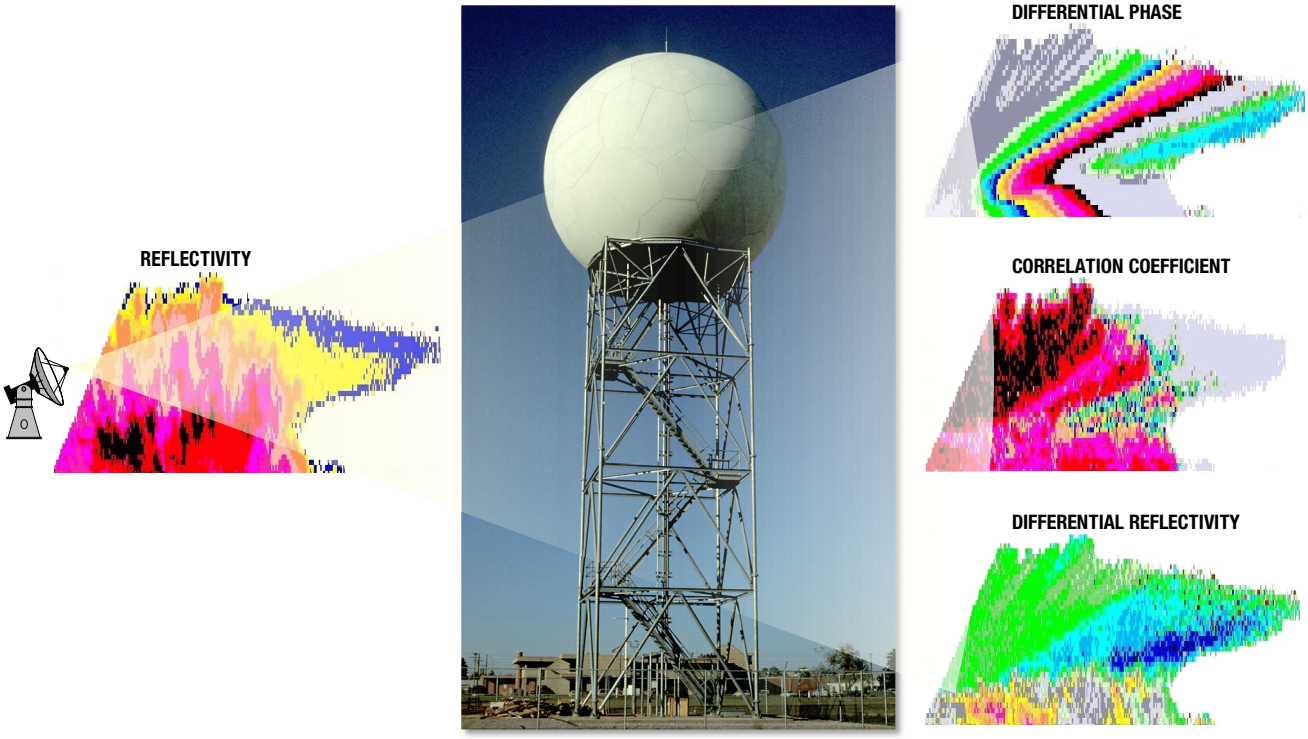

Calibration and Performance Analysis of NSSL's Polarimetric WSR-88D

V. M. Melnikov, D. S. Zrnić, R. J. Doviak, and J. K. Carter

May 15, 2003

National Severe Storms Laboratory
1313 Halley Circle
Norman, Oklahoma 73069

CONTENTS

PREAMBLE

Over the years NSSL has been providing technical information to the National Weather Service. This exchange had many forms, from formal reports and algorithms to consultation and supply of radar data in real time to the local Weather Services Forecast Office. After the decision to evolve its network of WSR-88Ds to keep pace with emerging knowledge and technology the NWS provided a spare WSR-88D to NSSL. Hence, NSSL became the principal NOAA Laboratory for evolutionary and revolutionary enhancements of weather radar science and technology. At that time (mid nineties) the NSSL Doppler Radar and Remote Sensing Research group committed to document in report form all significant innovations, changes, and results deemed of special value for operational applications regardless weather such reporting was formally required. This is the eleventh report in the series since 1997. It deals with engineering evaluation of the polarimetric upgrade of the research WSR-88D that took place concurrently with the first phase of the Joint POLarization Experiment (JPOLE) starting in spring of 2001. Many people contributed to this upgrade. Allen Zahrai led the team of engineers who designed the new processor which enabled scanning strategies and allowed more flexibility than the old system. Mike Schmidt and Richard Wahkinney made extensive modifications of microwave circuitry and controls. In the process, Mike became an integral, inseparable, and indispensable part of the system. Alexander Ryzhkov made numerous suggestions concerning data quality and vigilantly pursued this issue to perfection. Terry Schuur was the force behind the planning document for JPOLE. Alan Sigia, from Sigmet, resolved numerous technical details needed to operate the RVP7 processor in dual polarization mode. The NWS Radar Operations Center (ROC) contributed the basic RVP7 processor and display, which was subsequently enhanced to process dual polarization signals. Funding by the FAA over the last few years is gratefully acknowledged. Furthermore this is the first year that NWS specifically and generously contributed to the dual polarization effort at NSSL.

May 2003 in Norman
Dusan S. Zrnic

1. Introduction

This report describes the calibration procedures and engineering tests of the recently upgraded Research and Development WSR-88D radar. The radar, the first production model of the WSR-88D, was upgraded to have polarimetric capability to improve rainfall estimation, to classify precipitation types, and to differentiate weather echoes from those returned from biological scatterers (Doviak, et al; 1998). The main feature of NSSL's R&D polarimetric WSR-88D is the simultaneous transmission and reception of horizontally (H) and vertically (V) polarized waves , rather than the alternate transmission of H and V waves. The alternate transmission mode, which requires the use of an expensive ferrite switch, was implemented on earlier research polarimetric radars. The simultaneous mode does not require the switch, and improves the accuracy of the polarimetric measurements. To receive vertically polarized waves, a second receiver has been added (Fig. 1.1). This receiver has the same components as the WSR-88D receiver which normally receives H waves.

An interim solution has been implemented to process the polarimetric data, and provide a proof-of-concept of the polarimetric upgrades to the WSR-88D. This interim solution utilizes a commercial-off-the-shelf dual channel multiplexer developed by SIGMET (2002) whereby a single high speed digitizer is used to digitally convert the simultaneously received H and V signals[1]. In this case the H and V signals are required to have different intermediate frequencies. The planned long term solution for the WSR-88D is to have two high speed digitizers converting H and V signals that are at the same intermediate frequency. The implementation of the interim processing scheme has been made, and tests were conducted to determine the quality of the polarimetric upgrade to the WSR-88D. A detailed technical description of the interim system, as currently implemented on NSSL's R&D WSR-88D is given by Doviak, et. al. (2002). Here we report on the results of these tests.

We describe several techniques that were used to calibrate the polarimetric variables obtained from the R&D WSR-88D, and to evaluate their performance. Some of these techniques have been developed for the non-Polarimetric WSR-88D. Toward the goal of calibrating the polarimetric WSR-88D, we used:

- test signals,
- solar radiation,
- external RF transmitters
- precipitation, and
-ground scatterers.

---

[1]Besides providing a quicker evaluation of the polarimetric performance of the WSR-88D, the interim solution was implemented to have the radar ready for the Joint Polarization Experiment, JPOLE, that started in the Spring of 2002.

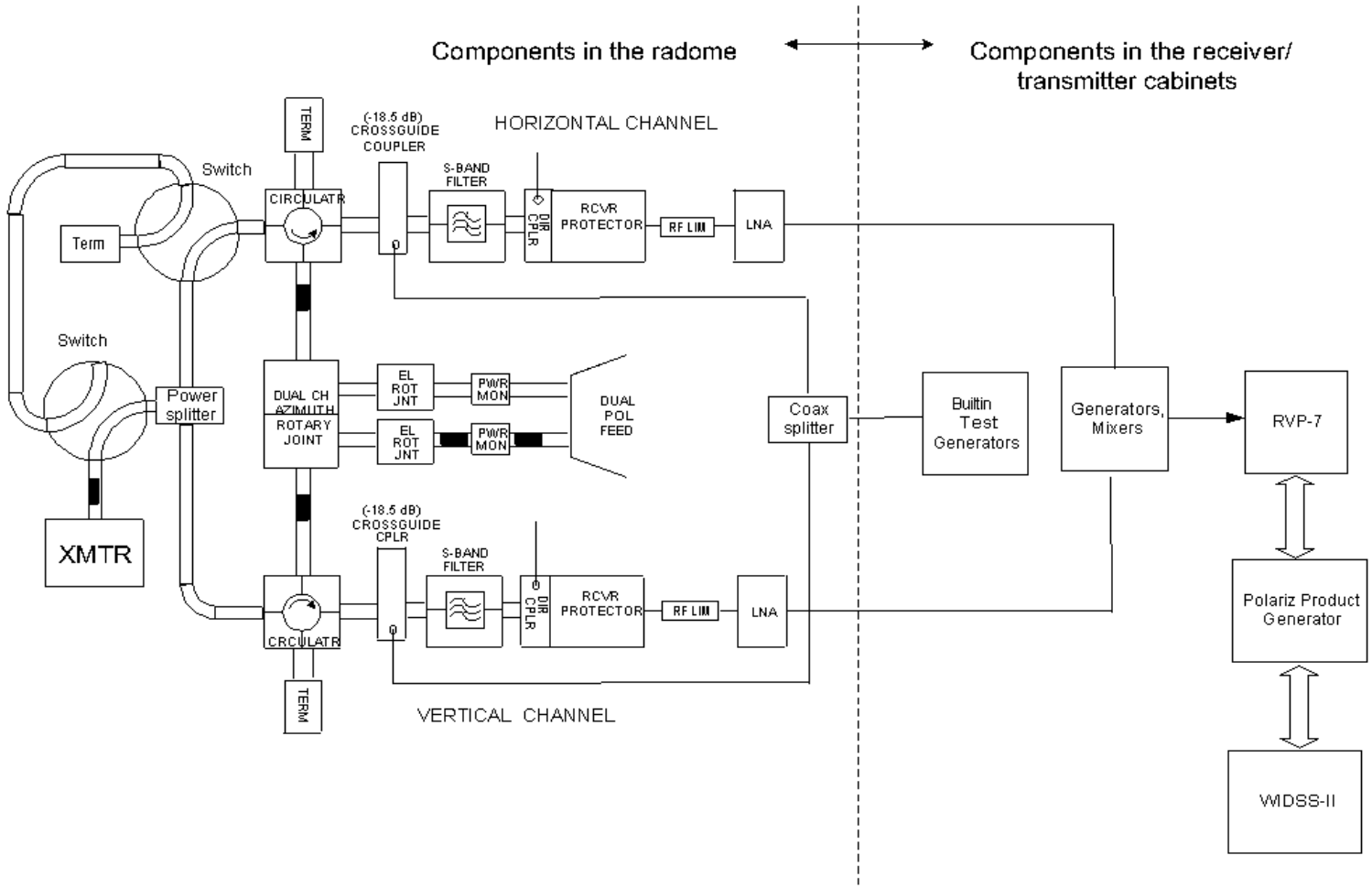

Fig. 1.1. System configuration for polarimetric measurements on the NSSL's research WSR-88D

Flexible waveguide Computer Local Area Network XMTR : Radar Transmitter

LNA : Low noise amplifier WDDS-II: Warning Decision Support System Integration Information

An additional method of calibrating a radar is to measure the backscatter cross section of a metal sphere that is lifted aloft by a negligibly reflecting balloon [Atlas, 2002]. We have not implemented this approach because echoes from the sphere are often contaminated by echoes from the ground (i.e., ground clutter). Further more, flying balloons at sufficiently high altitudes, to decrease the magnitude of echoes from the ground, requires special permission from the FAA. This is not practical for routine calibration of the radar.

2. Short technical description of the dual-pol R&D WSR-88D

The radar simultaneously transmits and receives horizontally and vertically polarized waves. A high voltage power splitter is used to form two transmitting channels in the R&D WSR-88D (Fig. 1.1). To process vertically polarized waves, a second receiver, identical to the existing one, has been added. A commercial (SIGMET RVP7) processor is passively connected to the radar to allow testing of the system, and to process H and V signals, without affecting the normal (i.e., legacy) operations of this WSR-88D. This processor requires combining two offset IF signals, one for the H the other for the V channel. We have retained the initial 57.5490 MHz intermediate frequency (IF_H) of the legacy H channel, and have designed circuits to generate a 63.3039 MHz intermediate frequency (IF_V) for the V channel. The IF_V frequency is generated using a newly designed interface (Doviak, et. al. 2002) between the WSR-88D's analog circuits and the RVP7 digital receiver/processor.

NSSL's R&D WSR-88D can operate in two polarization modes: 1) the Simultaneous transmission and reception of Horizontally and Vertically polarized waves (SHV) mode, and 2) the transmission of a linearly polarized wave (i.e., for the WSR-88D the polarization is horizontal), but simultaneous reception of both horizontally and vertically polarized waves (Depolarization mode). In the SHV mode, the following variables are available from the RVP7 processor:

1) reflectivity factor Z_h,
2) Doppler velocity v,
3) spectral width σ_v,
4) differential reflectivity Z_{DR},
5) the magnitude of the complex correlation coefficient, ρ_{hv}, between copolar voltages (i.e., the received H signals from transmitted H waves, and the received V signals from transmitted V waves), and
6) the differential phase shift φ_{dp} (i.e., the argument of the complex correlation between the copolar voltages).

Doviak and Zrnic [1993] rigorously define all these variables. The first three variables Z_h, v, and σ_v are exactly the same as those obtained from non polarimetric Doppler radars such as the legacy WSR-88D.

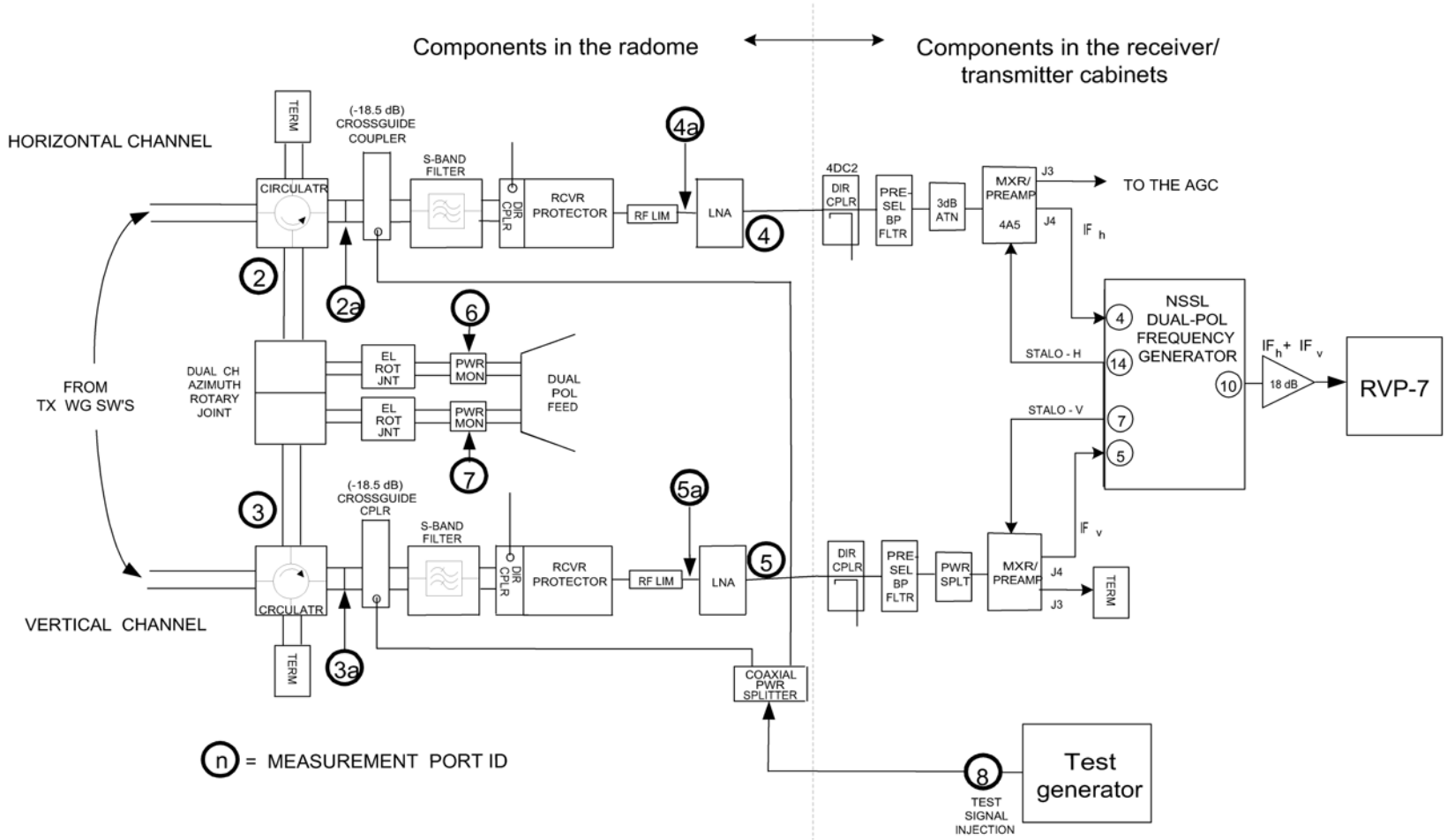

Fig. 3.1. Block diagram of the dual-pol system. Locations where calibration and measurements were made are indicated.

The second mode (i.e., Depolarization mode) is engaged to obtain depolarization data. Two waveguide switches in the transmit chain (Fig. 1.1) are used to bypass the power splitter so that only H waves can be transmitted. As in the SHV mode, both H and V waves are simultaneously received. The cross-polar (i.e., the received V signals when only H waves are transmitted) and co-polar signals are processed to compute

1) reflectivity factor Z_h,
2) Doppler velocity v,
3) spectral width $\sigma_{v,}$,
4) the linear depolarization ratio L_{DR},
5) the magnitude of the complex correlation coefficient ρ_h between the copolar and cross polar voltages, and
6) the phase φ_h of ρ_h.

In this mode the transmitter and the copolar receiver are identical to the WSR-88D; the second channel receives the cross polarized "V" waves.

The output data from the RVP7 are the above described variables from each resolution volume along the radar's beam. These variables are processed in the dual-pol product generator which is a distinct PC on the LAN. The dual-pol products are shipped to a PC with WIDSS-II (Weather Information and Decision Support System- Integration Information) software to display the polarimetric variables as well as the three Doppler spectral moments. The output dual-pol products can be found on the web at: www.nssl.noaa.gov/users/hondl/public_html/radar

3. Bandwidth of the R&D WSR-88D and the RVP7 frequency response

The two IF signals, IF_h and IF_V, are sampled with the RVP7's digital IF receiver (RVP7 User's Manual, 2002). The digital receiver performs best with a receiver noise bandwidth that is larger than the signal bandwidth (Zrnic, 2001). Because the RVP7 digital receiver has a sampling frequency (i.e., f_s = 35.9752) much lower than the two IF frequencies, the digital receiver under-samples the signals. Although bandpass digital filters in the RVP7 are used to separate the H and V samples, the receiver will also respond to H and V signals at frequencies far removed from IF_V and IF_H as we will shortly demonstrate. The effects of these out-of-band signals, that are aliases of IF_V and IF_H, have to be considered. For example, to calibrate the radar using wideband solar signals, and to correct the measured polarimetric parameters for noise, we need the frequency response of the digital receiver to these out-of-band signals as well as the bandwidth of the radar's analog components.

We begin with the measurements of the bandwidth of the microwave components. Fig. 3.1 shows the radar configuration which was used for the majority of the measurements described in this report. To measure the microwave bandwidth of this interim R&D polarimetric WSR-88D from the output of its microwave circulators to the output of its low noise amplifiers, the WSR-88D's built-in RF noise generator was used. This path includes a waveguide filter that was designed to reject signals that are outside the nominal bandwidth of the NSSL's WSR-88D and, in particular, the radar transmissions from KCRI, an operational testing WSR-88D radar

located a few hundred meters away. This filter likely dominates the bandwidth of all the microwave components in the R&D WSR-88D.

To amplify the noise generator's signal, a wideband TWT amplifier (HP 491C) was added to the output of the noise generator. The spectra were recorded with an HP 8563A Spectrum Analyzer that was first connected to the input of the radar receiver (i.e., the test signal injection port 8 in Fig. 3.1) to measure the spectrum of the signals at the output of the TWT, and then at the output from the Low Noise Amplifiers (i.e., LNAs at ports 4 and 5 in Fig. 3.1). The spectrum of the input signal (i.e, the output from the TWT) is presented in Fig. 3.2; it shows a relatively uniform output in the band from 2.67 to 2.74 GHz that surrounds NSSL's WSR-88D's transmitter's frequency (i.e., 2705 MHz). The change in level of the TWT's spectrum is less than 1 dB across this band. This noise spectrum was the input to the H and V radar receivers. The output spectrum from the H channel LNA is also presented in Fig. 3.2 with a thick line. The 3 dB bandwidth is about 30 MHz and the 30 dB bandwidth is about 43 MHz. Results for the V channel are almost identical.

The spectra at the output from the H and V mixer/pre-amplifiers (i.e., at ports 4 and 5 in Fig. 3.1) are shown in Fig. 3.3. The 3 dB bandwidths of the filters located at the two IF frequencies are 10 MHz, a bandwidth that is set by a bandpass filter in the Dual-Pol Frequency Generator (Doviak et al., 2002). Because the noise bandwidth is about 10 times the signal bandwidth, the dynamic range of the digital receiver can be increased by about 10 dB (Zrnic, 2001).

The digital receiver takes the place of several analog receiver components (i.e, the phase detectors, the video amplifiers, the AGC circuitry, and the analog matched filter). Because the Nyquist frequency is much lower than the IF_H and IF_V frequencies, and because the analog bandwidth of the IF signals is relatively large (i.e., 10 MHz), the digital receiver responds to signals over a very large bandwidth as we now demonstrate.

A simplified block diagram of a digital receiver is sketched in Fig. 3.4a. The RVP_7 digital receiver uses a single Analog-to-Digital Converter (ADC) that samples, at a frequency f_s, the combined H and V analog signals, $s_H(t) + s_V(t)$ that are at their respective IF frequencies, IF_H and IF_V. The RVP7 digital receiver under-samples the signals and passes all the aliases of IF_H and IF_V that are within the bandwidth of the analog components. That is, the H-digital filters pass all the frequencies that are aliases of $s_H^{(f)}$, where $s_H^{(f)}$ is the alias within the Nyquist band from zero to $f_s/2$ (Fig. 3.4b). Because the signals are real, the alias are those signals whose spectrum is *folded* about zero frequency and $f_s/2$, and integer multiples of $f_s/2$ as shown in Fig. 3.4b for the H and V channels of the digital receiver. The aliases (vertical dashed lines) are spaced $\Delta f_H = 3.586\text{MHz}$ about odd integers of $f_s/2$ for the H channel, and are spaced $\Delta f_v = 8.646\text{MHz}$ about

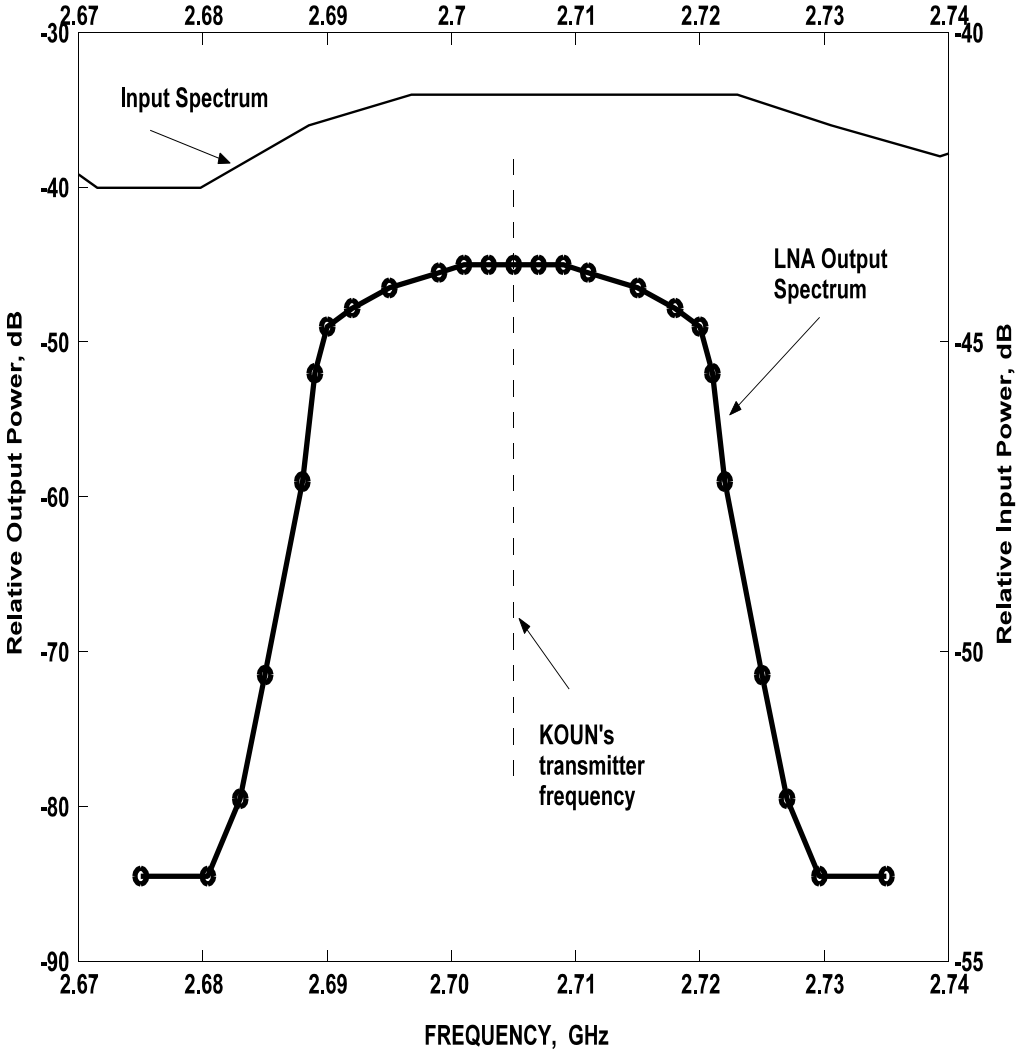

Fig. 3.2. Radar frequency response at RF and input spectrum of the noise generator. The right vertical scale is for the input signal to the LNA, the left vertical line is for the output signal from the LNA.

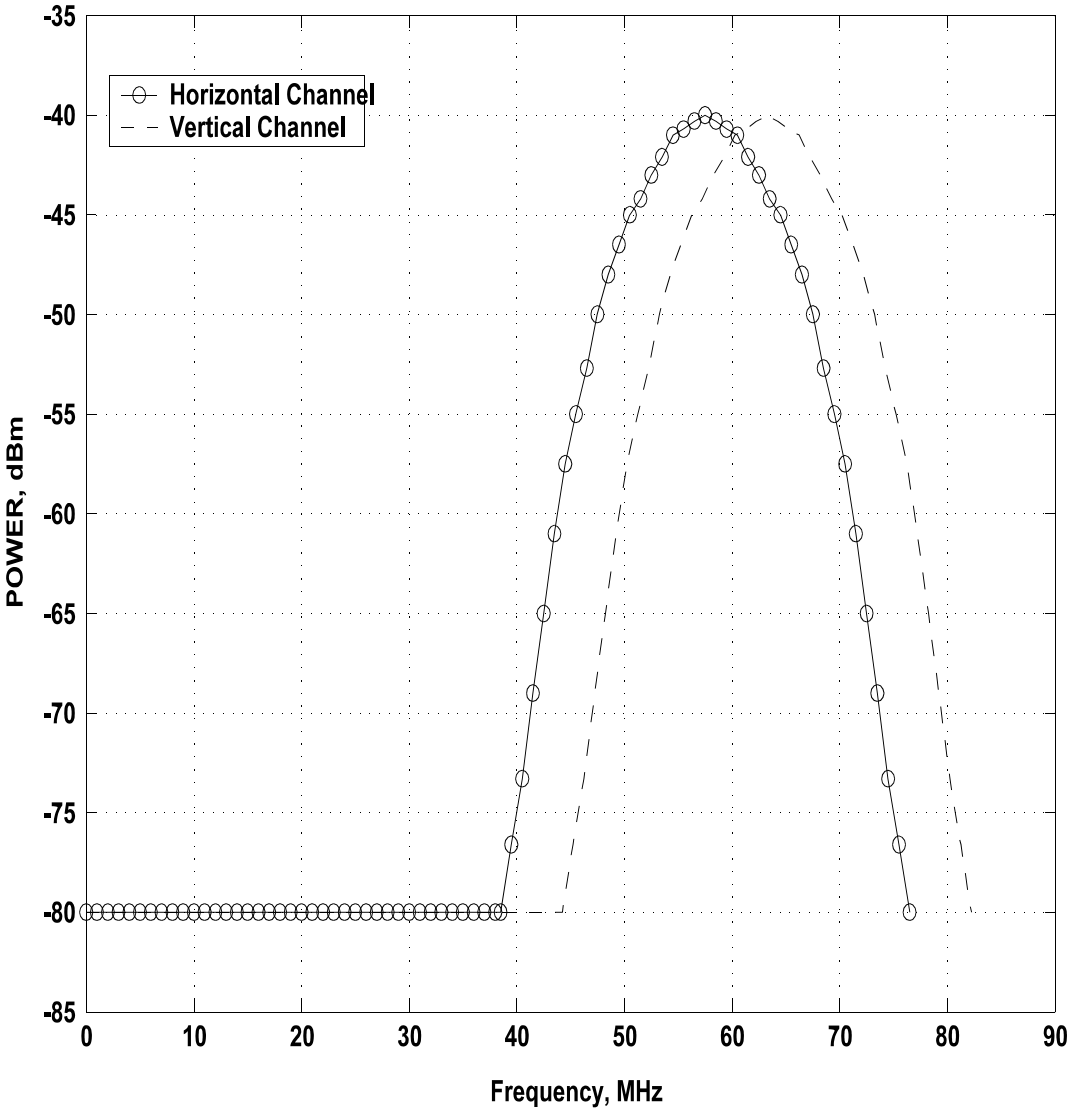

Fig. 3.3. Frequency responses of the IF channels. The IF frequence in the horizontal channel is 57.55 MHz and in the vertical channel it is 63.30 MHz.

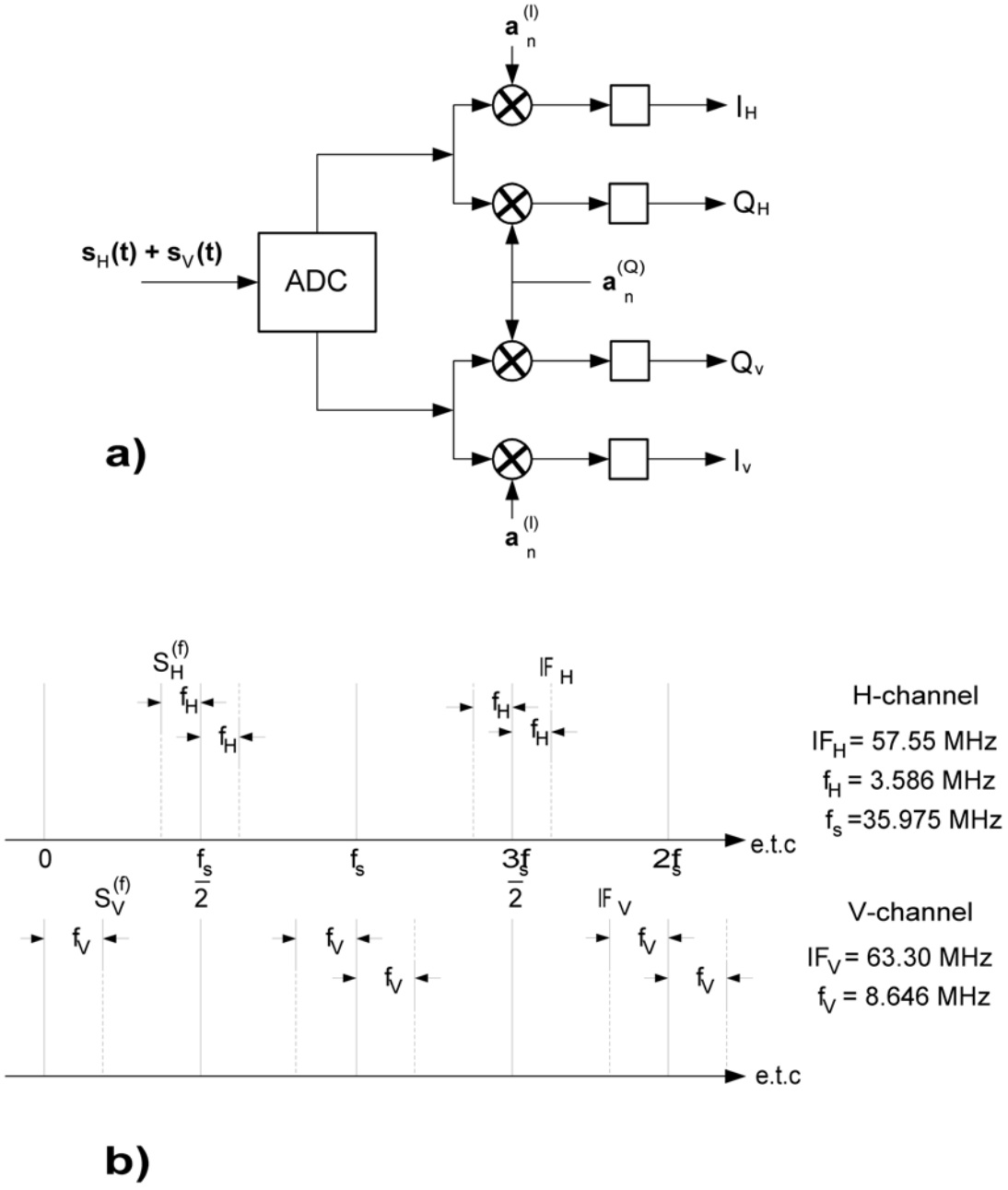

Fig. 3.4. Simplified block diagram of a digital receiver (a) and the frequency layout for the H- and V-channels (b).

even integers f_s/2for the V channel. Analog anti-aliasing filters (i.e., filters with bandwidths much smaller than those currently used in the analog chain) can be applied in the analog signals in the H and V channels to limit the signals to a relatively small band of frequencies about IF_H and IF_V respectively. For example, an anti-aliasing filter with a bandwidth of about 7 MHz centered on IF_H could significantly decrease the response to the frequencies about IF_H-$2\Delta f$. However, anti-aliasing filters were not included. The responses of the RVP7 digital receiver to the aliases of IF_H and IF_V has been verified and quantified through simulation and experiments. First we discuss the simulation of the RVP7's receiver response assuming there are no filters preceding the ADC in Fig. 3.4a.

Let $s(t) = s_H(t) + s_v(t)$ be the combined IF output signals from the mixers (Fig. 3.1) which are the input to the digitizer. The ADC (Fig. 3.4a) with the sampling frequency f_s outputs digital samples $s_n = s(n\tau_s)$, where n is an integer and $\tau_s = 1/f_s$ is the time interval between adjacent samples of $s(t)$. These samples are digitally filtered to separate the H and V samples, and then passed to a digital synchronous detector (i.e., multiplier) and low pass filter which convert the signals to the baseband In-phase, I, and Quadrature-phase, Q, digital samples. The digital synchronous detector multiples the filtered digital signals with a precalculated series of $a_n^{(I)}$ and $a_n^{(Q)}$ weights, and the low pass filter sums a number N of the multiplier products to compute the I and Q signal components (RVP7 User Manual, 2002; section 5.1.1):

$$I = \sum_{n=0}^{N-1} s_n a_n^{(I)}, \qquad Q = \sum_{n=0}^{N-1} s_n a_n^{(Q)}, \tag{3.1}$$

where

$$a_n^{(I)} = l_n \sin\left[\frac{\pi}{4} + 2\pi\frac{F_{IF}}{f_S}(n - \frac{N-1}{2})\right],$$

(3.2)

$$a_n^{(Q)} = l_n \cos\left[\frac{\pi}{4} + 2\pi\frac{F_{IF}}{f_S}(n - \frac{N-1}{2})\right], \qquad n = 0..N-1.$$

The values of the precalculated coefficients, l_n , and the number N used in the sum can, if properly selected, form a filter matched to the transmitted pulse.

In the simulations, an H signal $s_H(t) = A\sin(2\pi ft)$ with f between 30 to110 MHz was used in Eq. 3.1, whereas $F_{IF} \equiv IF_H$ in Eq. 3.2 is fixed at 57.54 MHZ, N = 50, and a Gaussian

function was used to calculate the values of l_n. The calculated power (i.e., $I^2 + Q^2$) is plotted in Fig. 3.5 as a function of *f*. These results are consistent with those sketched in Fig. 3.4.

To measure the actual frequency response of the RVP7, an external test signal generator (i.e., HP 8648 C) was used. A constant level of IF signal power was applied at Port 10 of NSSL's Dual-Pol Frequency Generator (Fig. 3.1). The output of the RVP7 was measured as a function of the signal generator's frequency *f* as it varied from 43 to 87 MHz. The results of these measurements are presented in Fig 3.6. Similar results were found for the V channel. By comparing simulated results in Fig. 3.5 with results from experiments (Fig. 3.6) we see that measurements and simulations are in close agreement. The frequency response of the H analog components, taken from Fig. 3.3, is also shown in the figure (black thick line). Thus the combined frequency response of the digital and analog receivers would be the product of the two responses sketched in Fig. 3.6.

As can be deduced, the combined receiver response suppresses, by more than 60 dB, the signal alias about $\frac{(2m+1)}{2} f_s$ for $m \neq 1$. But the alias signal at the window $\frac{3}{2} f_s - \Delta f_H$ (i.e., at 50.45 MHz) is only suppressed by about 5 dB. Therefore signals can pass through this spectral window to contribute significantly to the output power. For example, wideband signals like noise and the solar emissions will contribute powers through both spectral windows. Section 4 has a discussion on how the spectral window at 50.45 MHz affects noise and solar radiation measurements and calibration.

For wideband noise such as that generated by solar emissions and receiver noise, the noise bandwidth is approximately equal to the 3 dB width of the frequency response. For the V channel the analog filter suppresses, by more than 35 dB, those signals within the window aliases relative to signals at IF_V = 63.3MHz. From Fig. 3.6 we see that the 3 dB width is about 0.83MHz and thus the noise bandwidth B_v is about 0.83MHz. On the other hand, the noise bandwidth of the H channel is larger because the window alias at 50.38MHz is only suppressed by 5 dB relative to signals within the spectral window at IF_H = 57.55MHz. Thus the noise bandwidth B_h of the H channel calculates to be about 1.09MHz. Thus the noise power in the H channel receiver should be 1.2 dB larger than that in the V channel. Measurements of noise power reported in section 9 of this report verify this calculation.

One can see from Fig, 3.6 that the Z_{DR} , which is the ratio of H channel output power to V channel output power, is a large positive dB value, as expected, when a signal at frequency *f* is within the H channel spectral windows (e.g., at 50.45, 57.55, and 86.35 MHz) of the H channel, and likewise Z_{DR} is negative when *f* is within the two spectral windows of the V channel. At all other frequencies, the Z_{DR} is an quasi random oscillatory function. Because the digital filters are not perfect, some H and V signals pass to the outputs of the H and V channels where the ratio of powers is computed. This is likely the cause of the oscillatory-like Z_{DR} values, but it appears that,

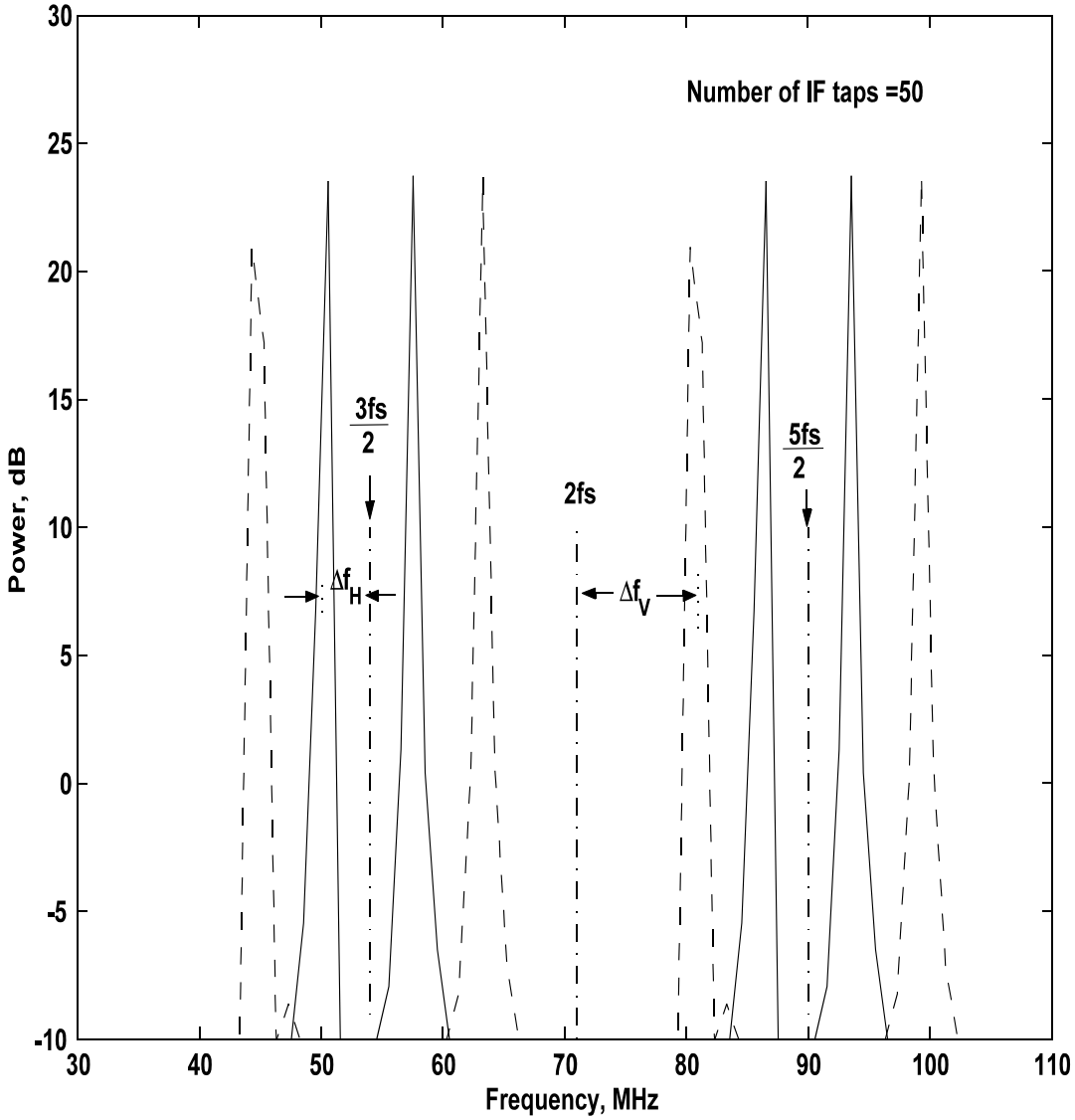

Fig. 3.5. Simulated frequency response of the RVP7.

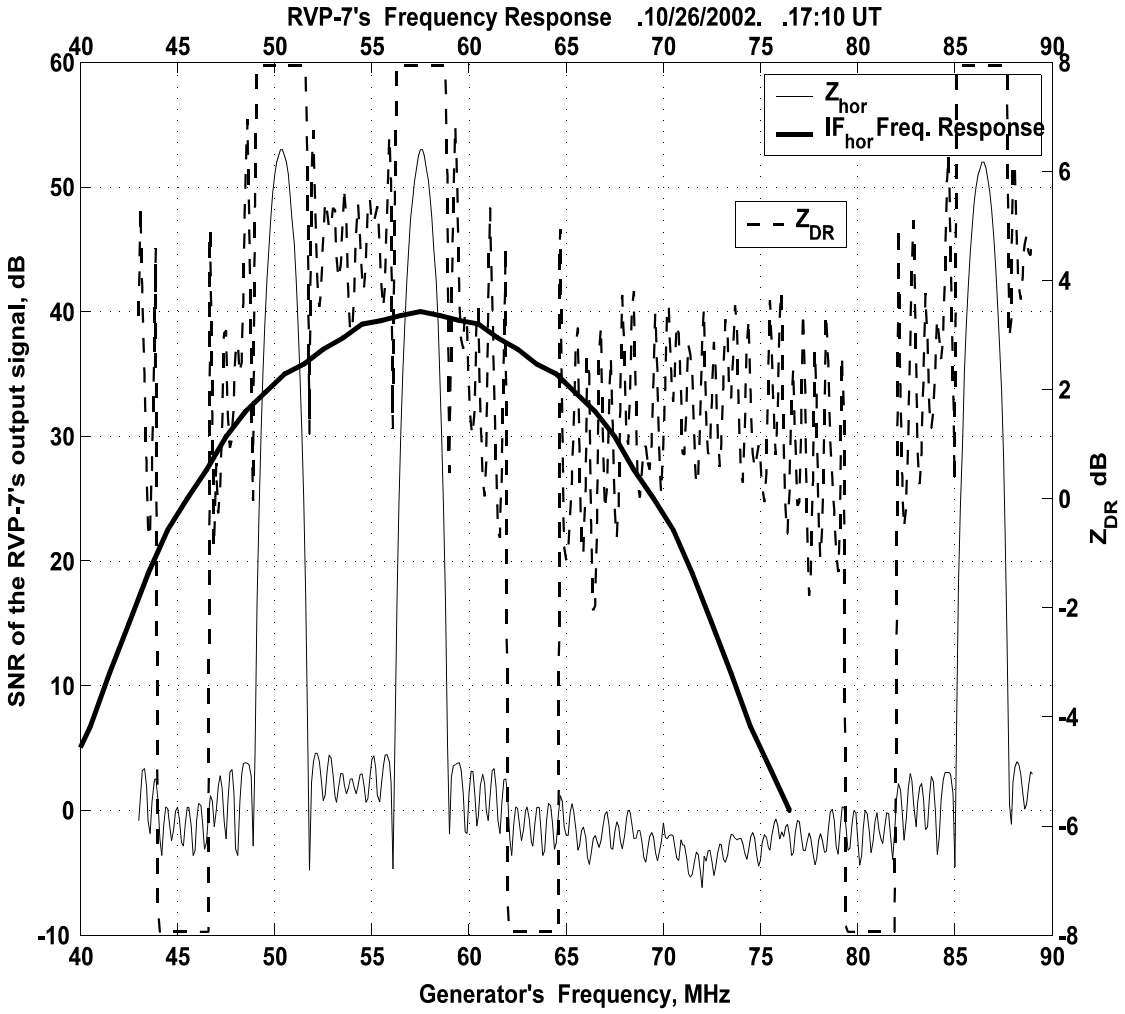

Fig. 3.6. Frequency response of the RVP7 measured in the H channel (thin line) and Z_{DR} (dashed line). The thick line is the frequency response for the H channel

on average, more H than V power is passed to the output of the RVP7. From Fig. 3.6, it can be seen that the H channel digital bandpass filter suppresses, by about 53 dB, any signals in the H channel that are at frequencies within the IF_V = 63.30 MHz spectral window of the V channel.

Because power at the alias spectral window f = 50.45 MHz will be transferred to the output, although with 5 dB attenuation relative to the power at $f = IF_H$ = 57.55 MHz , the processor will have positive Z_{DR} bias for wideband signals such as receiver noise or solar emissions, even if the H and V receivers have their gains matched. Furthermore, because the noise bandwidths of the H and V receivers are not matched, it is shown in section 4 that if noise alone is present, the Z_{DR} is about 1 dB, and not 0 dB as it should be. We will also see a bias in solar radiation measurements described in section 4. The Z_{DR} for wideband signals measured with the RVP7 varies from 1 dB to 2.2 dB.

We conclude that receiver noise and solar radiation measurements made with the RVP7 are affected by the frequency response of the combined analog and digital filters and that these effects are not matched for the H and V receivers. Analog anti-aliasing filters at the input to the RVP7, or a digital filter at the output of the ADC, with center frequencies midway between the IF_H and IF_V frequencies, and with a bandwidths slightly larger than the difference between the two IF frequencies, would help to diminish this effect.

4. Polarimetric parameters and measurements

Before developing and discussing the calibration methods, let's first review the signal processing used in the RVP7 to estimate the polarimetric parameters, and briefly discuss the relation between the polarimetric parameters measured with the RVP7 and the hydrometeors' intrinsic polarimetric parameters. These intrinsic parameters are defined in terms of the scattering matrix, and are the quantities sought with radar measurements. The RVP7 also has options (e.g., noise corrections; offsets, etc.) that the user can select, and the selection can impact the calibration. Noise correction is complicated by the fact that noise power is strictly not a constant, but depends on the beam pointing angle.

4.1 Signal processing in the RVP7

In the RVP7 processor, all polarimetric parameters for each resolution volume are calculated using the I and Q digital signals (3.1) at the output of the H and V channels. The I and Q signal components in each channel form a pair of complex digital voltages V_h and V_v,

$$V_h = I_h + jQ_h, \qquad V_v = I_v + jQ_v \tag{4.1}$$

The number N of samples or taps used in the sum in Eq. (3.1) for each resolution volume determines the response time of the digital low pass filter. The number of taps $N = 30$ provides a response that is matched to the 1.57 μs width of the transmitted pulse for the short-pulse mode of the WSR-88D. To calculate the polarimetric parameters, M samples are processed during the dwell time (i.e., M times the PRT). The number M depends on required accuracy of measurements, and determines the antenna rotation rate, and/or the azimuthal angular resolution. In our measurements we used $M = 64$, 128, and 256. The number $M = 256$ is the largest number that can be processed by the RVP7, and it was used in the calibrations described below.

An important part of calibration consists of gain measurements for the H and V receivers, as well as the differential phase shifts within the radar. These measurements are used to determine offsets (e.g., differential gain offsets, etc.) that added (as an option in the RVP7) to the polarimetric parameters (e.g., $Z_{DR(m)}$, $L_{DR(m)}$, etc.) to compensate for differential phase shifts and gains within the radar. As part of the calibration tests we also determined the stability of the differential gains and phase shifts.

As mentioned in the introduction, NSSL's R&D WSR-88D can operate in either the SHV or Depolarization mode. In either of these modes, measurements and calculations are made using the signals at the output of the H and V receivers (i.e., at the input to the RVP7; Fig. 3.1). Although we imply two outputs, the outputs are physically in the same cable (i.e., the cable that carries H and V signals at different IF frequencies) connected to the RVP7. Thus, when we use the term powers $P_h^{(0)}$ and $P_v^{(0)}$ at the output of the H and V receivers, we refer to the powers at the input to the RVP7.

In terms of the complex digital voltages, the output powers are:

$$S_h^{(0)} + N_h^{(0)} = P_h^{(0)} = \frac{1}{M}\sum_{m=1}^{M} V_h^{(0)}(m)V_h^{(0)*}(m) \qquad S_v^{(0)} + N_v^{(0)} = P_v^{(0)} = \frac{1}{M}\sum_{m=1}^{M} V_v^{(0)}(m)V_v^{(0)*}(m) \tag{4.2}$$

where $S^{(0)}$ and $N^{(0)}$ are the signal and noise powers at the receiver's output, and the super-scripted asterisk denotes a complex conjugate.

4.2 Relation between polarimetric parameters and RVP7 measurements

The intrinsic polarimetric parameters such as Z_{dr} , L_{DR}, etc. are defined in terms of the elements of a covariance matrix (Doviak and Zrnic, 1993, Section 8.5) which is determined by the scattering properties of an ensemble of hydrometeors. For example, the differential reflectivity factor Z_{dr} is defined as,

$$Z_{dr} \equiv \frac{Z_h}{Z_v} = \frac{<|s_{hh}|^2>}{<|s_{vv}|^2>} \tag{4.3}$$

where s_{hh} and s_{vv} are elements of the backscattering covariance matrix and are proportional to the copolar backscatter cross section of a hydrometeor (Doviak et al., 1998, Section III.1.1). The brackets indicate an ensemble average of the hydrometeor's properties (e.g., size, canting angle, etc.). For example, if there is a distribution of sizes of spherically shaped hydrometeors, the average is over the distribution of sizes and $<|s_{hh}|^2>$ will be proportional to the expected backscatter cross section of a hydrometeor. These ensemble averages are also referred to as the bulk properties of the scatterers within the resolution volume. The sub-scripting notation used here is consistent with Doviak and Zrnic (1993). The first subscript index designates the polarization of the wave in the receiving channel, and the second subscript index refers to the polarization of the transmitted signal that produced the received signal.

But measurements are made of backscattered signals at the output of the radar receiver, and these must be related to the elements of the covariance matrix. This is the purpose of calibrating the radar. For example, assuming spherical water drops and Rayleigh scatter, the reflectivity factor $Z = Z_{hh} = Z_{vv} \propto <|s_{hh}|^2>$ is related to the signal power $S^{(0)}$ at the output of the receiver as (Doviak and Zrnic, 1993, Section 4.4.5),

$$Z = \frac{2^{10}(\ln 2)\lambda^2 r_0^2 \ell^2 \ell_r}{\pi^3 P_t g^2 g_s \theta_1^2 c\tau |K_w|^2} S^{(0)} \tag{4.4}$$

where all units are in the MKS system, θ_1 (radians) is the one-way half-power width of an

assumed circularly symmetry radar beam, g is the gain(dimensionless) of the antenna, g_s is the system gain, c the speed of light, τ is the transmitted pulse width, $K_w \approx 0.93$ for liquid water is related to the refractive index of water, r_0 is the range to the resolution volume which contains the scatterers contributing to the range-gated weather signal sample, λ is the radar wavelength, ℓ is the one-way atmospheric attenuation, and ℓ_r is the loss in output power due to the finite bandwidth of the receiver. All parameters in Eq. (4.4) are referenced to a common point, typically the receiver's input or antenna port. Thus the system gain is the net gain from the antenna port to the receiver's output, the transmitted power P_t is, as well, that at the antenna port. Although measurements of weather signal power and receiver noise are made at the output of the receiver, and transmitted power often at some other point in the radar, the measured voltages must be expressed in terms of the signals, noise, and transmitted power at a common port. In the case of the WSR-88D this is at antenna ports 6 and 7 in Fig. 3.1.

Furthermore, because the transmitted powers in the H and V polarized waves can be different, adjustments to the measured powers must be made to account for differences in transmitted powers. For example, the power in the vertically polarized waves transmitted by NSSL's R&D WSR-88D is about 1.023 (0.11dB) times more than that in the horizontally polarized wave. Differences in transmitted power are principally caused by losses in the H and V circulators, and in the H and V channels of the azimuthal rotary joint. Although the differences in loss factors are quite small, the relative powers need to be monitored and adjustments made to insure that the measurements account for differences in transmitted powers. Furthermore, the gains, g_h and g_v, of the H and V receiver channels might not be the same, and these also have to be monitored and adjustments made to the output measurements to insure that the signals referenced to the antenna ports are properly calculated; this is the purpose of the calibration. On the other hand, calibration typically does not take into account other significant problems, such as differential attenuation along the path, effects of canting angle, etc. (Doviak et al., 1998) that need to be addressed in order to relate measurements to the backscattering covariance matrix; these are problems that are addressed by other means (e.g., online or offline computers that operate on signal processor's output).

To estimate polarimetric parameters at low signal-to-noise ratios *S*/*N*, noise measurements need to be made and these also need to be referenced to the antenna port. Because the WSR-88D uses low-noise amplifiers at its input, the noise contributions are from two sources: 1) the internal noise of the receiver, and 2) external radiation from ground, sky, and precipitation. Although noise corrections, to obtain signal power from the signal plus noise power, are available as an option in the RVP7, we have chosen not to implement this online correction feature because the WSR-88D noise power is a function of elevation angle (Fig. 4.1) and whether the radar is or is not pointed at a storm (Fig. 4.2). Thus, under certain circumstances, noise corrections need to be more rigorous, and these can be best done offline.

To obtain the data in Fig. (4.1), the transmitter was turned off and the output power of the H channel was recorded as a function of elevation angle for angles from about -1.5° to about 10°.

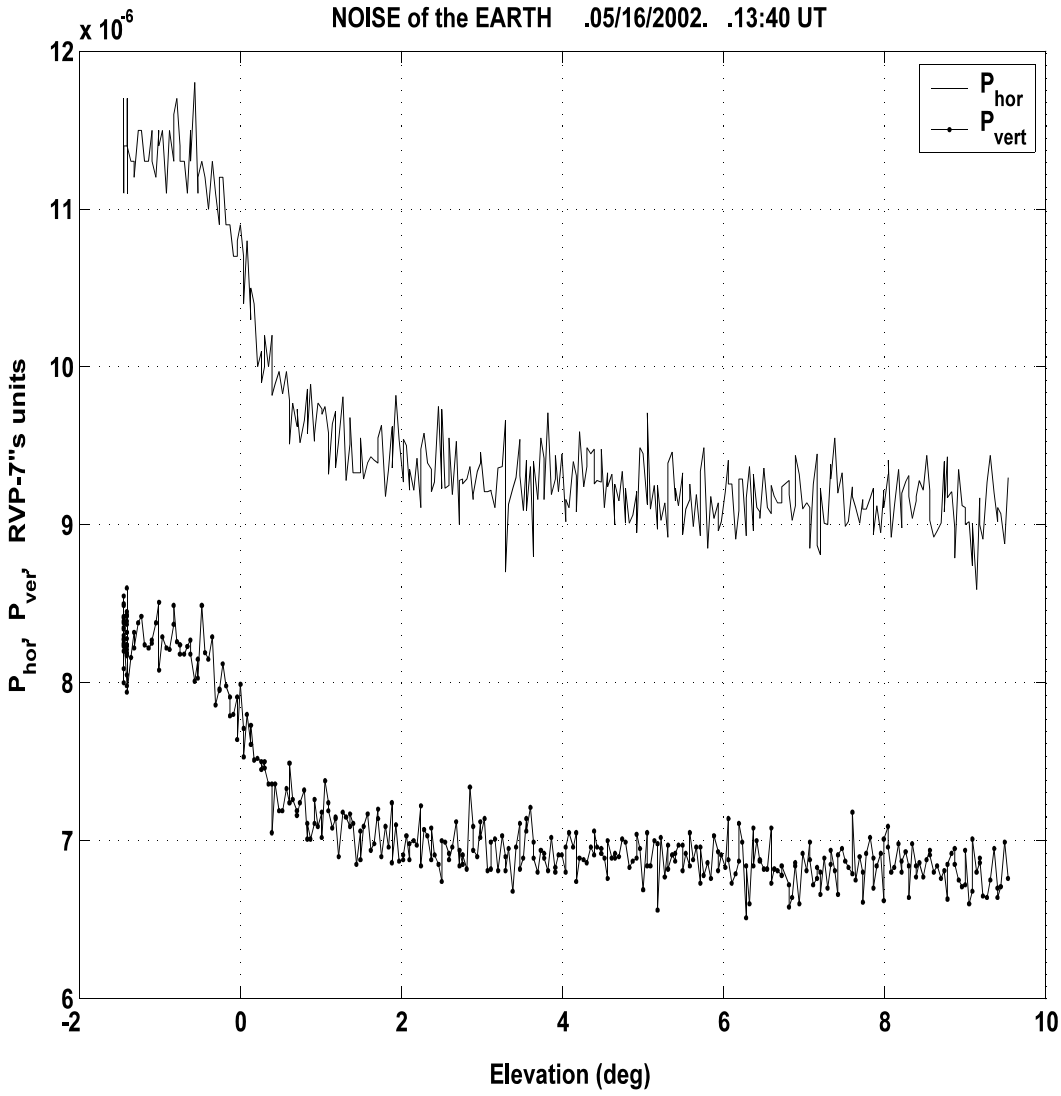

Fig. 4.1. Elevation dependence of system noise in the H and V channels. System noise consists of internal radar noise and external Earth's noise.

At the lowest elevation angles, the radar beam is directed at the ground which emits broadband noise because it is a warm body (temperature≈290K), that is much hotter than that of the effective temperature (≈25K) of the sky (Doviak and Zrnic, 1993, Section 3.5.1). Sky radiation is only resolved by the radar when the beam is elevated above 1 or 2°. Fig. 4.1 shows the ground and sky noise power as a function of elevation angle revealing about a 0.7 dB change between noise levels if the beam is directed at the horizon versus that received if the beam is directed at the clear sky. Adjustments for noise power are more complicated than if the noise level was fixed. So data for calibration has been collected with the RVP7 without using its online real time corrections. This correction is made off line, and days and elevation angles are chosen where noise power from external sources is relatively constant.

As part of the calibration procedure, the differential phase shifts between H and V channels must be measured. In the following sections we show how measurements at the output of the RVP7 receiver/signal-processor are related to the various polarimetric variables (i.e., differential reflectivity, copolar correlation coefficient, etc), which are defined in terms of the covariance matrix elements.

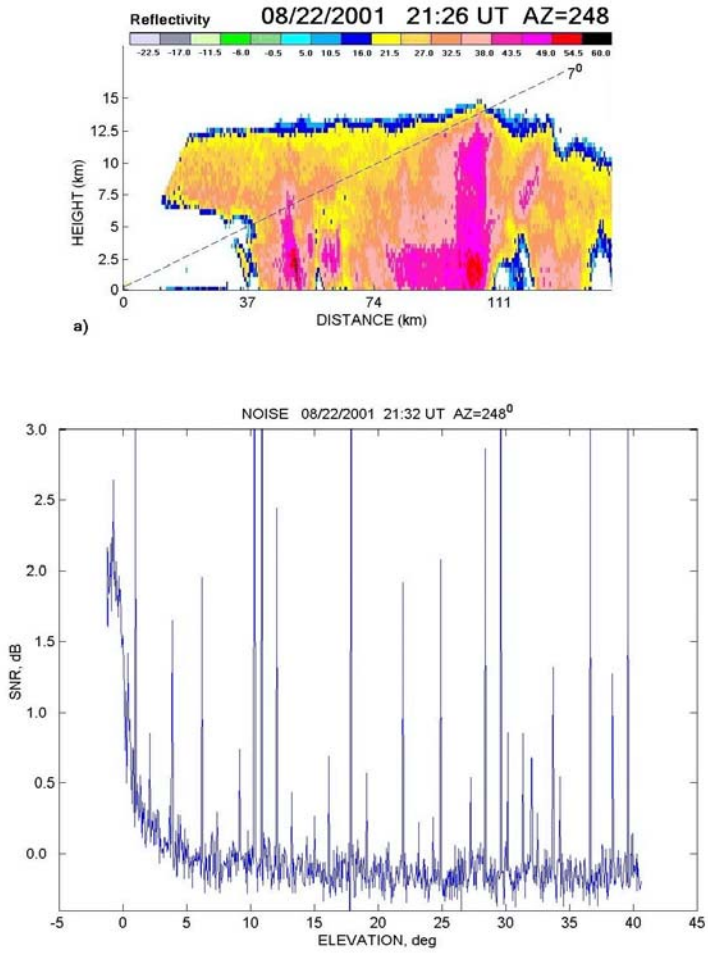

Fig. 4.2. Reflectivity vertical cross section (a) and the elevation dependence of system noise with significant contribution from cloud's thermal noise (b). Vertical spikes in (b) are from lightning discharges. Relative noise power is with respect to noise when the antenna is pointed at high elevation.

5. Differential reflectivity factor Z_{dr} calibration

To measure differential reflectivity, the radar is operated in the SHV mode. The purpose of Z_{dr} calibration is to derive factors that correct the decibel ratio of power at the outputs of the H and V receivers to estimate the intrinsic Z_{dr} of the scatterers. Correction factors associated with differences in receiver gains can be obtained by applying equal powers from narrow band generators to the antenna ports 6 and 7 (Fig. 3.1). But measurements at ports 6 and 7 are not practical for routine calibration because these ports are above the rotary joints. Equal levels of power from the generator can be more conveniently applied to the receivers through cross guide couplers which are connected to ports 8 which are below the rotary joints. Moreover, the injection of calibration signals into ports 8 can be done periodically and frequently during data collection (e.g., at the end of volume scans as is done in the legacy WSR-88D). But this measurement does not account for losses from the antenna ports to the cross guide couplers. These losses need to be measured separately. Fortunately, these losses should not change in time, and thus do not require frequent measurement, as do the active components such as low-noise amplifiers, receiver protectors, etc.

Alternatively, equal levels of wide band signal power can be passed to the antenna ports (i.e., ports 6 and 7) by directing the antenna's beam toward the sun which emits equal amounts of spectral power density in both H and V waves. In either case (i.e., using narrow-band signal generator power, or wide-band solar power), derived correction factors only account for differences in receiver gain. Furthermore, because the bandwidths of the H and V channels of the digital receiver are different (Section 3), the solar power in the H and V channels will differ. This difference in bandwidths further complicates derivation of correction factors for the receiver. To obtain correction factors that account for differences in both receiver gains and bandwidths, as well as differences in transmitted powers, measurements of transmitted powers at ports 6 and 7 are required. On the other hand, correction factors for differences in receiver gains and transmitted powers can be obtained directly by making observations of appropriate weather signals. For example, Z_{dr} can be calibrated using observations of drizzle and clouds for which there is confidence that Z_{dr} is unity (i.e., Z_{DR}(dB) = 0). In this section we report on several methods used to calibrate Z_{dr}.

Ignoring attenuation along the propagation path, it can be shown that the intrinsic differential reflectivity factor Z_{dr} is related to the measurements of powers, $P_h^{(0)}$ and $P_v^{(0)}$, at the output of H and V channels of the RVP7 receiver as,

$$Z_{dr} = \frac{g_v}{g_h \delta_t} \frac{g_{av}^2}{g_{ah}^2} \frac{(P_h^{(0)} - N_h^{(0)})}{(P_v^{(0)} - N_v^{(0)})} \tag{5.1}$$

where g_h , g_v are the gains in the H and V channels from the antenna port to the output of the receiver, g_{ah}, g_{av} are the antenna gains, $\delta_t \equiv P_h^{(t)} / P_v^{(t)}$ is the ratio of the H and V powers transmitted in the SHV mode, and $N_h^{(0)}$ and $N_v^{(0)}$ are the noise powers at the output of the H

and V channels. The following derivations and discussion assume that the antenna gains for H and V polarized waves are matched (Doviak, et al., 2000) and we omit these gains. For reasons discussed earlier, noise powers are not subtracted from the output power when data is collected for meteorological observations. That is, the signal plus noise power is recorded and corrections for noise are made during offline processing. Thus to compute Z_{dr} offline, the relative gains of the H and V channels must be known, as well as the differences in the transmitted powers. In addition, if noise powers cannot be ignored, the output noise powers need to be measured and recorded. It is common and convenient to express the differential reflectivity in decibel units. Thus Eq. (5.1) can be written as,

$$Z_{DR} = 10\log Z_{dr} = G_v - G_h - \Delta_t + 10\cdot\log\frac{P_h^{(0)}}{P_v^{(0)}} + 10\cdot\log\frac{1-(N_h^{(0)}/P_h^{(0)})}{1-(N_v^{(0)}/P_v^{(0)})} \qquad (5.2)$$

where G is the receiver gain expressed in decibel units, and $\Delta_t \equiv 10\log\delta_t$. Because noise power and signal power are amplified equally, Eq. (5.2) can be expressed in terms of the input (i.e., at the antenna port) signal-to-noise ratios, $(S_v / N_v)^{(i)}$ and $(S_h / N_h)^{(i)}$ as,

$$Z_{DR} = G_v - G_h - \Delta_t + 10\cdot\log\frac{P_h^{(0)}}{P_v^{(0)}} + 10\cdot\log\frac{1-(N_v/S_v)^{(i)}}{1-(N_h/S_h)^{(i)}} \qquad (5.3)$$

If one uses the RPV-7 option of not correcting for noise (SIGMET, 2002, Section 5.7.6), as is done for meteorological observations using the RVP-7, the logarithm of the output power ratio will give the correct Z_{DR} value only if the S/N is sufficiently high, and receiver gains and transmitted powers are matched. The fourth term is the "measured" differential reflectivity factor, $Z_{DR(m)}$, and is the parameter that is recorded for offline calibration and engineering analysis. The first three terms combined are called the system differential reflectivity, $Z_{DR\,SYS}$, because if true Z_{DR} (i.e, the decibel ratio of weather signal power at the antenna port) is 0 dB, and S/N is high, $Z_{DR(m)}$ will register the system differential reflectivity.[2] The last term, labeled $Z_{DR\,SNR}$, is the change in the measured differential reflectivity factor , $Z_{DR(m)}$, caused by finite S/N . Thus, Eq. (5.3) can be written as

$$Z_{DR(m)} = Z_{DR\,SYS} + Z_{DR} + Z_{DR\,SNR} + Z_{DR\,OFF} \qquad (5.4)$$

where

$$Z_{DR(m)} = 10\log\frac{P_h^{(0)}}{P_v^{(0)}} \qquad (5.5)$$

[2] This definition is reciprocal to that used by SIGMET (2002, p. 5-46) by defining $Z_{DR\,SYS} \equiv GDR = 10\log(g_v/g_h\delta_t)$.

$$Z_{DR\,SYS} = G_h - G_v + \Delta_t\,, \tag{5.6}$$

$$Z_{DR\,SNR} = 10\log\frac{1-(N_h/S_h)^{(i)}}{1-(N_v/S_v)^{(i)}}\quad . \tag{5.7}$$

The last term in Eq. (5.4), called the differential reflectivity offset, $Z_{DR\,OFF}$, has been added because it is a parameter within the RVP7 that is assigned values to adjust or correct the offsets or $Z_{DR(m)}$ biases due to differences in receiver gain and transmitted power, but not biases due to noise power. If $Z_{DR\,OFF}$ is set to be equal to the negative of $Z_{DR\,SYS}$, Eq. (5.4) reduces to

$$Z_{DR(m)} = Z_{DR} + Z_{DR\,SNR}\quad . \tag{5.8}$$

It can be shown that in order to ignore noise powers, and to maintain an accuracy better than 0.2 dB in the Z_{DR} measurements of rain, where Z_{DR} is generally positive and can be as large as 4 dB, a SNR higher than 15 dB is required. Thus noise corrections for real time observations are necessary unless data having SNR < 15 dB are not displayed; otherwise meteorological interpretation will be compromised.

Because cross-polar signals are mixed with copolar signals when the radar is operated in the SHV mode (required to obtain Z_{DR} data), Eq. (5.3) would, strictly speaking, have to account for these cross-polar signals. But, hydrometeors, particularly raindrops, typically contribute very little cross-polar power compared to the copolar power. Maximum cross-polar power is no more than about 10dB below copolar power. Such high values of cross-polar power is limited to unusual conditions such as that found in the melting layer for moderate to light rains (Doviak and Zrnic, 1993, Table 8.1). By avoiding such unusual conditions, the contribution from the cross-polar signal can be ignored in calibrating Z_{DR}.

5.1 Z_{DR} calibration using test signals

Consider Z_{DR} calibration that can be done with test signals and measurements of transmitted powers. The procedure consists of two steps: 1) measurement of the system differential reflectivity in-receive, i.e. G_h - G_v, and 2) measurement of the system differential reflectivity in-transmit, i.e. Δ_t (see Eq. (5.6)).

5.1.1 Calibration of the system differential reflectivity in-receive

To obtain the system differential reflectivity in-receive, i.e. to obtain $Z_{\text{DR SYS}}^{(\text{R})}$, test signals from the built-in radar signal generator can be used. Consider strong signals with the signal-to-noise ratios more than 30 dB. In this case, we can neglect $Z_{\text{DR SNR}}$ in Eq. (5.4) and should substitute $Z_{\text{DR SYS}}$ with $Z_{\text{DR SYS}}^{(\text{R})}$ because the transmitter is not used in this stage of calibration. The signal from the built-in CW generator is injected at port 8 (Fig. 3.1) and is supplied to two crossguide couplers in the H and V channels. The signal power can be measured at ports 2a and 3a (before the crossguide couplers) with a power meter and the ratio of the H power divided by power in the V-channel was 1.02. This is due of slightly different cable lengths and not equal outputs from the coax power splitter. The crossguide couplers have different attenuations. Using the manufacturer's specifications we obtained the ratio of the attenuations in the H and V-channels of 1.03. We set the programmable offset, i.e. $Z_{\text{DR OFF}}$, to zero so that Eq. (5.4) can be written as

$$Z_{DR(m)} = Z_{DR\ SYS}^{(R)} + Z_{DR(coplers)} + Z_{DR\ SIG} \tag{5.9}$$

where $Z_{DR\ SIG}$ is measured power ratio 1.02 expressed in dB, i.e. 10log(1.02) = 0.09 dB, and $Z_{\text{DR(couplers)}}$ is a value reciprocal to the obtained ratio of attenuations expressed in dB, i.e. -10log(1.03) = - 0.13 dB. The measured $Z_{\text{DR(m)}}$ was -0.33 dB. So $Z_{DR\ SYS}^{(R)}$ is

$$Z_{DR\ SYS}^{(R)} = -0.33 + 0.09 - 0.13 = -0.37dB \tag{5.10}$$

Strictly speaking, the measured $Z_{DR\ SYS}^{(R)}$ is not the whole system differential reflectivity in-receive because the circulaters, the rotary joints and the antenna are out of the measurement paths. But the circulators and the rotary joints have attenuations about 0.1 dB so that the relative attenuation is smaller than that. The antenna has differential gain very close to 0 (Doviak et al., 2000) so that the value of (5.10) can be considered as a good estimate for the system differential gain in-receive.

5.1.2 Transmitted power differences

The only term left for differential reflectivity calibration is $Z_{\text{DR SYS}}^{(\text{T})}$ (i.e., Δ_t in Eq. 5.3). This part of the system differential reflectivity is obtained by measuring transmitted powers at ports 6 and 7 (Fig. 3.1). These measurements are reported by Doviak, et al. (2002, p. 6[3]). In short

[3]Due to the use of an incorrect coupling factor for the direction coupler at port 7 (Fig. 3.1), the peak power (143 kW) reported in the cited report was incorrect.

$$P_h = 160 \text{ kW}; \quad P_v = 164 \text{ kW}; \ \therefore \quad \Delta_t = -0.11 \text{ dB}. \tag{5.11}$$

The measurements of P_h have the accuracy of 0.2 dB because the power meter has the accuracy of 0.1 dB and attenuator at port 6 (Fig. 3.1) can be calibrated with the accuracy of 0.1 dB. The same is for the vertical channel.

Thus the system differential reflectivity factor $Z_{DR\,SYS}$ is:

$$Z_{DR\,SYS} = G_v - G_h - \Delta_t = -0.37 - 0.11 = -0.48 \text{ dB} \tag{5.12}$$

5.2 Z_{DR} calibration using sun scans

Solar radiation measurements have been used in radar meteorology for a long time (e.g., Pratte and Ferraro 1989, 1995). In the legacy WSR-88D calibration, the sun scan data is used to determine the antenna gain and beamwidth. Here we describe only the results for Z_{DR} calibration, keeping in mind that we can only calibrate differences in the H and V receivers. One difficulty in using solar radiation to calibrate Z_{DR} is the lack of a capability to precisely direct the antenna's beam to the center of the solar disk and to maintain this track. The WSR-88D's antenna positioning system has an accuracy of 0.05^o in azimuth and elevation, and this level of accuracy is inadequate for Z_{DR} calibration. In our sun calibration procedures, we forced the antenna to make narrow azimuthal sector scans (i.e., 1.0^o) at a fixed elevation angle, and at a low azimuthal scan rate (i.e., $0.1^o\ s^{-1}$). The sun passes through scan plane while signals from the H and V channel outputs are recorded with the RVP7 processor.

An example of data collected in this mode is presented in Fig. 5.1. Relative time in the figure corresponds to the data record number. At time ~ 15 the radar captures the solar signal and begins to make the azimuthal scans at constant elevation. As can be seen from Fig. 5.1, the power, P_h , in the H channel varies up and down as the beam passes back and forth across the solar disk. The sequence of short double peaks is due to the fact that the center of the scan plane is not centered on the path of the sun. As the sun passes through the plane of scan, the peaks of P_h increase until a maximum is reached at the time ($\approx$150) that the center of the solar disk is on the plane of the scan. We can use the sun scan data to measure the system differential reflectivity on-receive (i.e., $Z^{(R)}_{DR\,SYS} = Z_{DR\,SYS} + \Delta_t$) and, as well, to check the alignment of the H and V beams (Section 12). But the use of solar radiation data to determine $Z^{(R)}_{DR\,SYS}$ is tricky and requires correction for the mismatches in the noise bandwidths of the two receivers, as we now show.

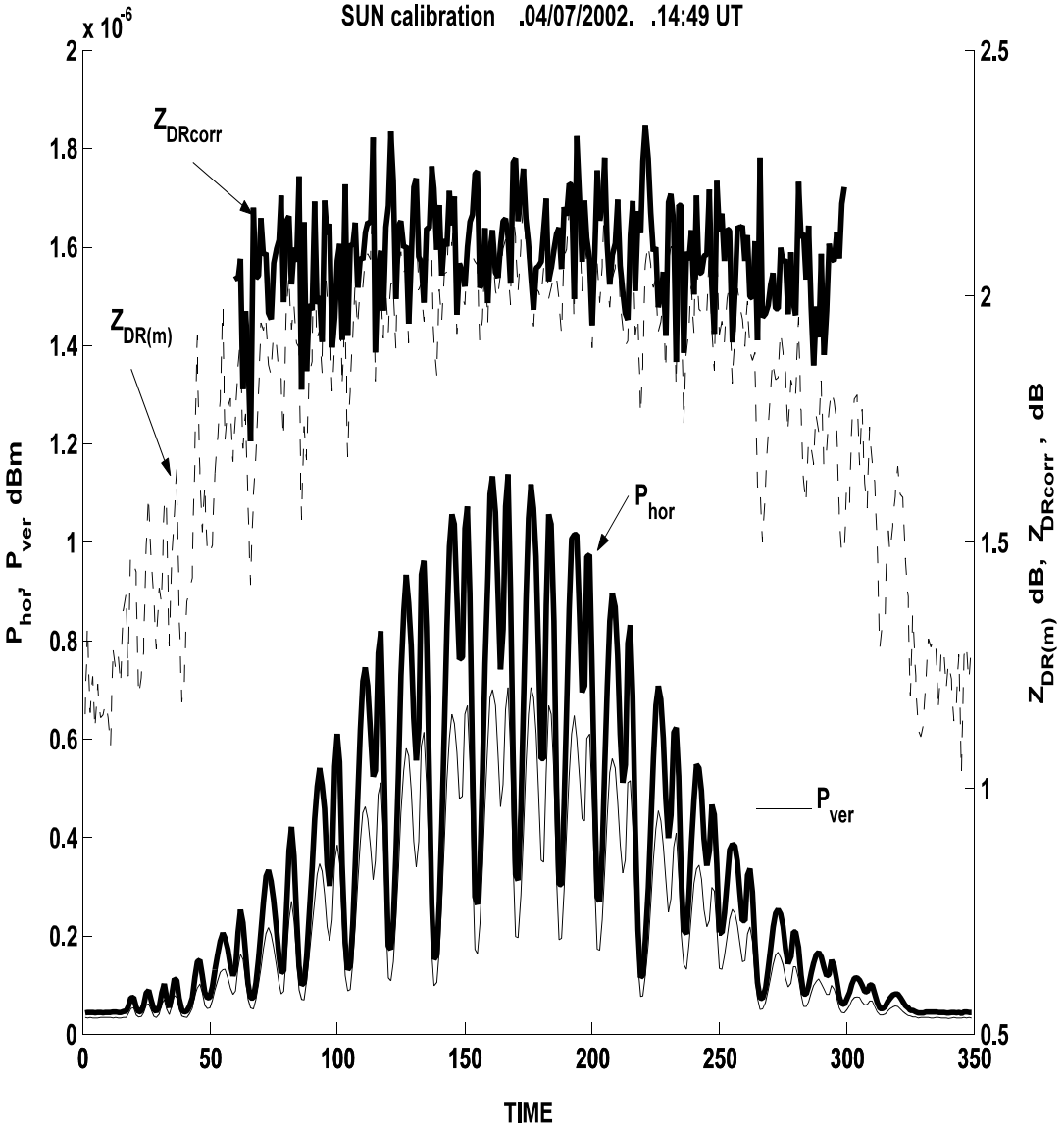

Fig. 5.1. Data recorded during sun scans on April 7, 2002..

5.2.1 Noise power corrections to solar $Z_{DR(m)}$

The sun radiates equal spectral power densities at H and V polarizations, so we can in principle, use observations of solar power to calibrate $Z_{DR\,SYS}^{(R)}$. Even though the spectral power density might be the same for H and V waves, the solar power $S^{(i)}$ referenced to the antenna port will likely be very different for the H and V channels because of the differences in the noise bandwidths (i.e., $B_h \neq B_v$; Section 3). Furthermore, there will be differences in noise power (e.g., emitting from external thermal sources). Noise power is principally from the Low Noise Amplifier (LNA; Fig. 3.1), and differences in the LNAs' noise temperatures, and the losses in the microwave components between LNAs and the antenna ports, can cause differences in the noise power referred to the antenna port. From Fig. 5.1, one can see that $Z_{DR(m)}$ (i.e., the log of the ratio of H and V output powers) depends upon the solar signal power. This is a result of the last term in Eq. (5.3); that is, $Z_{DR(m)}$ depends on the solar signal-to-noise ratio *S*/*N*. The solar signal is wideband noise generated by the sun. Note also that the solar signal power in H-channel is higher than the power in V channel (i.e., $Z_{DR(m)} > 0$). Part of this could be due to the fact that the gain in the H channel is larger than that in the V channel (i.e., $Z_{DR\,SYS}^{(R)} > 0$), and part is due to the larger noise bandwidth of the H channel as is stated in Section 3.

To correct the measurements for noise power when the sun is used as a source of radiation at the input to the receivers, we use Eq. (5.3) in which Z_{DR} is the logarithm of the ratio of the true solar signal power referred to the antenna ports. For solar emissions, the power spectral densities are equal (i.e., $S_h(f) = S_v(f)$), but the measured solar signal power referenced to the antenna ports is a function of receiver bandwidth. Because the noise bandwidth B_h of the H channel is not equal to the noise bandwidth B_v of the V channel, $S_h^{(i)} \neq S_v^{(i)}$. But because solar spectral densities are equal we find that

$$S_v^{(i)} = \frac{B_v}{B_h} S_h^{(i)} \tag{5.13}$$

Furthermore, because there is no transmitted power $\Delta_t = 0$ dB, and the differential signal of the sun computed as $Z_{DR\,(sun)}$ can be written as

$$Z_{DR}(sun) \equiv 10\log\frac{S_h^{(i)}}{S_v^{(i)}} = 10\log\frac{S_h(f)B_h}{S_v(f)B_v} = 10\log\frac{B_h}{B_v} \tag{5.14}$$

Substituting Eq. (5.14) into Eq. (5.4), and expressing the resulting equation in terms of $Z_{DR(m)}$, yields

$$Z_{DR(m)} = 10\log\left(\frac{g_h B_h}{g_v B_v}\right) + 10\log\left(\frac{1-\frac{N_h^{(i)}}{S_h^{(i)}}}{1-\frac{N_v^{(i)} B_h}{S_h^{(i)} B_v}}\right) \quad (5.15)$$

Noise powers $N_v^{(i)}$ and $N_h^{(i)}$ are not likely equal for two reasons: 1) $B_h \neq B_v$ and 2) the H and V LNAs could have different noise temperatures. It is easy to see from Eq. (5.15) that if receiver gains and noise bandwidths are matched, and receiver noise temperatures are equal, $Z_{DR(m)} = 0$, as expected.

We can rewrite Eq. (5.15) in the form

$$Z_{DRcorr} = 10\log\left(\frac{g_h B_h}{g_v B_v}\right) = Z_{DR(m)} - 10\log\left(\frac{1-\frac{N_h^{(i)}}{S_h^{(i)}}}{1-\frac{N_v^{(i)} B_h}{S_h^{(i)} B_v}}\right) \quad (5.16)$$

where Z_{DRcorr} is the differential reflectivity corrected by noise. The mean Z_{DRcorr} can be obtained from Fig. 5.1 and is 2.04 dB.

To obtain the ratio of gains in the channels, we have to obtain the ratio of the bandwidths in Eq.(5.16). The difference of the bandwidths is due to different frequency responses in the two channels (section 3). To measure the ratio of the bandwidths for wideband signals, we can apply the following scheme. Eq.(5.16) corresponds to the common connection of the radar channels and the RVP-7, i.e. the output from radar H-channel is connected to the RVP-7's input of H-channel (lower IF) and the output from radar V-channel is connected to the RVP-7's input of V-channel (higher IF). This connection corresponds to ports 4 and 5 at the NSSL's dual-pol frequency generator (see Fig. 3.1). We can switch over the radar channels at those ports, i.e. connect the H radar channel to port 5 of the generator and connect port 4 to the V radar channel. For this flipped connection we measure Z'_{DRcorr} which is according to (5.16) as follows:

$$Z'_{DRcorr} = 10\log\left(\frac{g_v B_h}{g_h B_v}\right) \quad (5.17)$$

From (5.16) and (5.17) we obtain:

$$G_h - G_v = 0.5(Z_{DRcorr} - Z'_{DRcorr}) \quad (5.18)$$

Z'_{DRcorr} for the measurements in Fig.5.1 is 2.61 dB so that

$$Z_{DR\,SYS}^{(R)} = G_h - G_v = 0.5(2.04 - 2.61) = -0.27\ dB \quad (5.19)$$

Thus it is seen that the H channel gain (including waveguide component losses and LNA and IF amplifier gains) from the antenna port to the RVP7 is 0.27 dB smaller than the gain in the V channel.

The only term left for differential reflectivity calibration is $Z_{\mathrm{DR\,SYS}}^{(\mathrm{T})}$ (i.e., Δ_t in Eq. 5.3). This part of the system differential reflectivity can be obtained by measuring transmitted powers at ports 6 and 7 (see 5.11). Thus the system differential reflectivity factor $Z_{\mathrm{DR\,SYS}}$ is:

$$Z_{\mathrm{DR\,SYS}} = G_v - G_h - \Delta_t = -0.27 - 0.11 = -0.38\ \mathrm{dB} \quad (5.20)$$

5.2.2 Solar Z_{DR} calibration stability

We used the solar radiation measurements to monitor the stability of $Z_{DR\,SYS}^{(R)}$ (i.e., the receiver's contribution to the solar Z_{DR}). Fig. 5.2 presents the results of the measurements during the period of May to December 2002. One can see from the figure that the variations of the measured solar $Z_{\mathrm{DR\,SYS}}$ lie in an interval of ±0.2 dB with a mean value of -0.3 dB so that

$$Z_{DR\,SYS}^{(R)} = -0.3\ dB \quad (5.21)$$

Adjusting $Z_{\mathrm{DR\,OFF}}$ we can reduce the mean errors of the $Z_{DR\,SYS}^{(\mathbf{R})}$ measurements to better than ±0.1 dB.

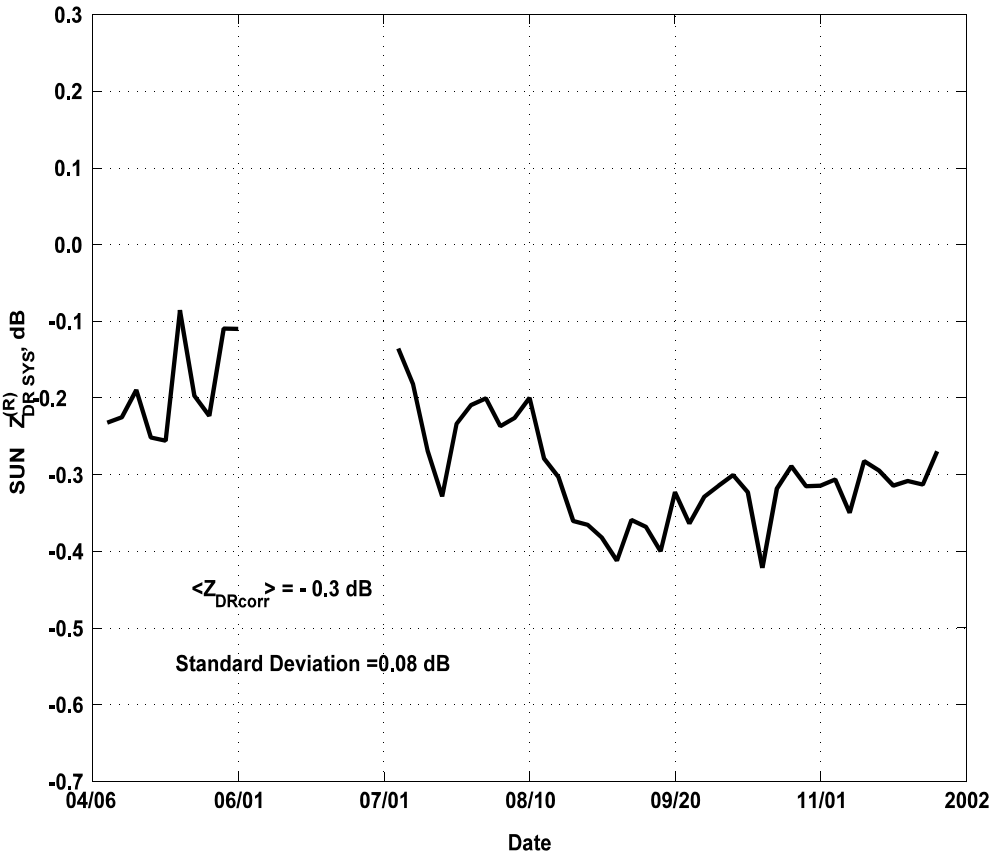

Fig. 5.2. Time variations of the $Z_{DR\ SYS}^{(R)}$ obtained from sun scans on dates indicated .

5.3 Z_{DR} calibration using weather signals

Z_{DR} calibration using solar radiation accurately determines the difference in the channel gains, but cannot account directly for differences in transmitted powers. But transmitted powers, as well as the system gains, can be measured and continually monitored by the WSR-88D during data collection. Z_{DR} calibration with appropriate weather can also provide an accurate assessment of the receiver gain and transmitted power differences. In many respects, the use of weather to establish Z_{DR} calibration is taken as crucial test. Certainly, if the weather scatterers are known to be spherical, the Z_{DR} measured must be zero, if not there are differences in receiver gains and transmitted powers which must be corrected, or offsets be added to the measured Z_{DR} (i.e,. $Z_{DR(m)}$) to adjust the displayed and/or recorded values. This is the purpose of adding an offset to the $Z_{DR(m)}$ as seen in Eq. (5.4).

Measurements at vertical incidence in rain are often used to establish the overall system bias of Z_{DR} (Bringi and Chandrasekar 2001, section 6.3.2). Because the rain drops are symmetrical in the mean for the vertical sounding, the intrinsic Z_{DR} is close to zero. This method, however, cannot be easily implemented with the WSR-88D because the beam has a 60° elevation limit determined by the structural configuration of the antenna's pedestal. Nevertheless, we discuss a Z_{DR} calibration method using weather signals received at the 60° elevation limit.

For low antenna elevations, stratiform rain such as drizzle can be used for Z_{DR} calibration. The particles in drizzle are practically spherical, and their intrinsic Z_{DR} is nearly zero. The echoes must be from volumes well below the freezing level in order to insure that there echoes from melting ice crystal aggregates do not contaminate the weather signals from drizzle. Furthermore, there needs to be confidence that large drops in the resolution volume do not significantly contribute to the weather signal from drizzle. This is hard to guarantee *a priori*. Despite these concerns, Z_{DR} calibration should be practical under conditions when drizzle echoes are expected to be the most significant contributor to the backscatter.

An example of Z, Z_{DR} , and ρ_{hv} data as a function of range for an elevation angle of 1° is shown in Fig. 5.3. At this elevation angle, observations at ranges less than 40 km will come from resolution volumes at heights below 800 meters. This is well below the melting level on this day. The melting level can easily be determined from the ρ_{hv} field. Because estimates of the polarimetric parameters are calculated from signals at the output of the receiver without correction for noise, noise power will bias the measurements. But it is not difficult to find regions where noise power and ground clutter do not bias the Z_{DR} measurements because both noise and ground clutter cause ρ_{hv} values to be significantly lower than 1.0. For example, ground clutter typically has ρ_{hv} values much less than 1.0, and noise powers larger than 20 dB below the signal power will cause the estimated value of ρ_{hv} to be less than 0.99. Thus, both the presence of ground clutter and noise can be identified by examining the correlation coefficient ρ_{hv}.

Based upon the previous discussion, we conclude that $Z_{DR(m)}$ measured without noise correction, should have values near zero in regions below the melting layer *provided* ρ_{hv} *is between* 0.99 and 1.00. One can see from Fig. 5.3 that there are several such regions. Among

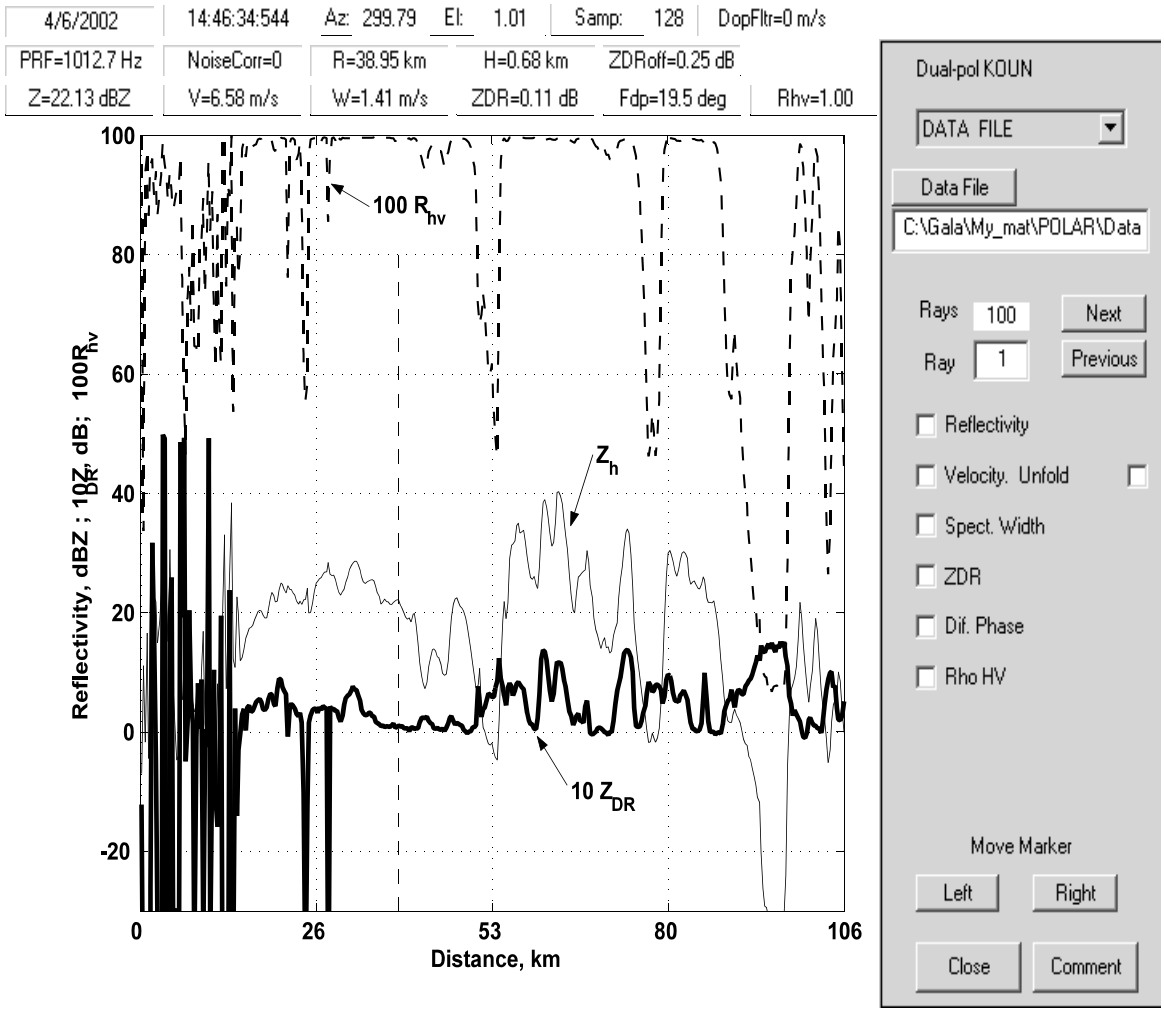

Fig. 5.3. Reflectivity, Z_{DR}, and ρ_{hv} profiles in drizzle. The elevation is 1^0.

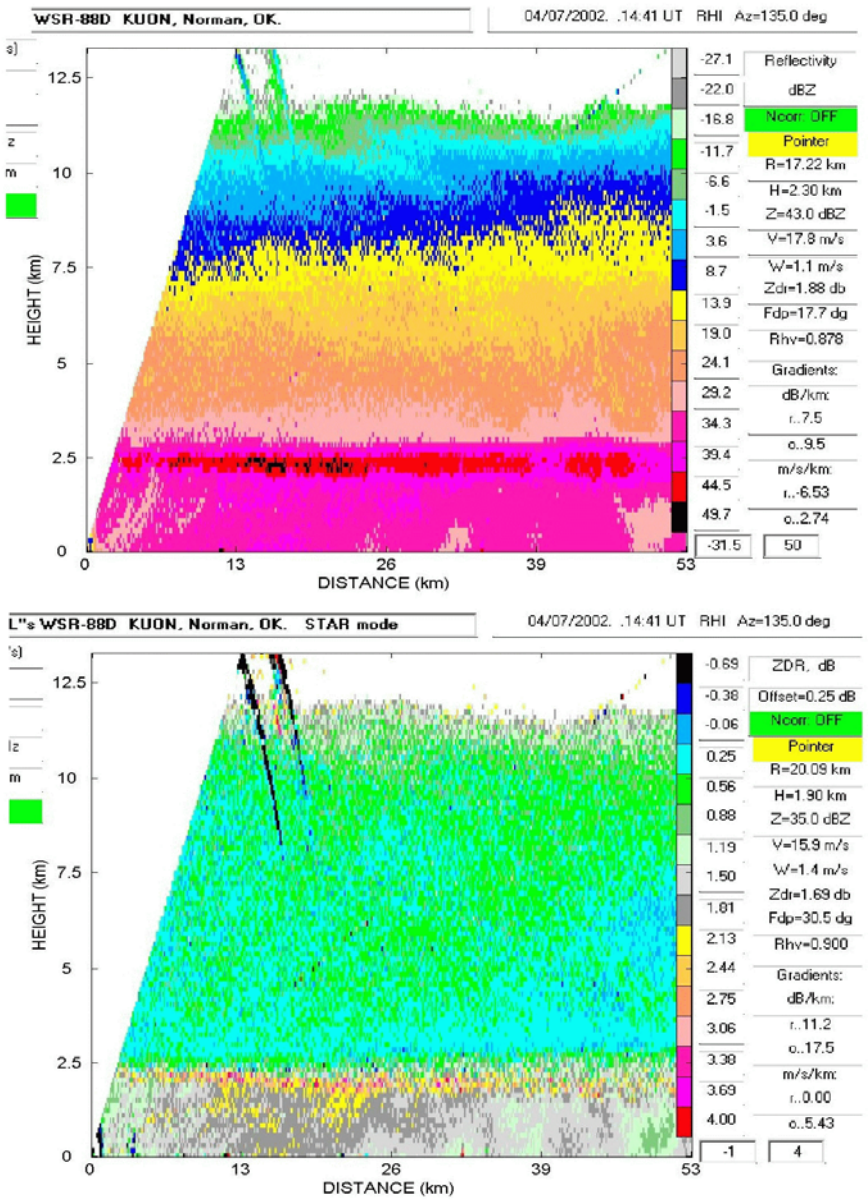

Fig. 5.4. The reflectivity (top) and Z_{DR} (bottom) fields. The $Z_{DR\ OFF}$ is 0.25 dB.

these regions one can choose a range interval having minimum Z_{DR}. This interval can be used to calibrate the system or offset differential reflectivity $Z_{DR\ OFF}$ (i.e., the appropriate correction factor required to convert the estimated Z_{DR} to obtain the intrinsic Z_{DR}). In Fig. 5.3 the region near the vertical dashed line at about 40 km is a good candidate. By varying $Z_{DR\ OFF}$, we made the measured Z_{DR} (i.e., $Z_{DR(m)}$) to be close to zero as seen in this figure. For the data presented in Fig. 5.3, the differential reflectivity offset $Z_{DR\ OFF}$ was set to +0.25 dB (see the data blocks at the top of this figure). From Eq. 5.4 we see that $Z_{DR\ SYS}$ must be set to $-Z_{DR\ OFF}$ to insure that $Z_{DR(m)} = 0$ when the intrinsic Z_{DR} is zero and *S/N* ratio is large. Thus, from drizzle observations we find that

$$Z_{DR\,SYS} = -0.25\ dB \tag{5.22}$$

Thus the output power in the H channel is larger than in the V channel. One can see from the figure that there are several intervals where measured $Z_{DR(m)}$ touches the zero line. By using this method for several radials of recorded drizzle data, we should be capable of calibrating Z_{DR} with accuracy better than 0.1 dB.

Comparing the system differential reflectivity offsets calculated from weather observations Eq. (5.22) with that in Eq. (5.21) derived from sun scan data we see about a 0.05 dB difference.

Measurements above the melting layer can, under certain circumstances, also be used for Z_{DR} calibrations. For example, oblate spheroidal particles with a mean vertical orientation, have a Z_{DR} that decreases with elevation as (Bringi and Chandrasekhar, 2001, sections 2.3.2 , 4.7.1):

$$Z_{dr}(\theta) \approx \frac{Z_{dr}(0)}{[Z_{dr}(0)^{1/2} \sin^2\theta + \cos^2\theta]^2} \tag{5.23}$$

where $Z_{dr}(0)$ and $Z_{dr}(\theta)$ are differential reflectivities at elevation angles of 0° and θ° respectively (Z_{dr} is expressed on a linear scale). Thus even though the maximum elevation angle for the WSR-88D is limited 60° it can be easily shown from the above equation that $Z_{dr}(\theta = 60°)$ is significantly less than $Z_{dr}(\theta = 0°)$. Above the melting layer, hydrometeors are usually frozen and dry, and thus their refractive index is significantly less than that of water drops. At elevation angles near 60°, the upper limit of angles for WSR-88D, it can be shown that $Z_{DR}(60°) < 0.24$ dB for scatterers having $Z_{DR}(0) < 1$ dB. That is, atmospheric scatterers with low values of intrinsic Z_{DR} could serve well for Z_{DR} calibration.

Dry aggregated snow is probably the best choice for differential reflectivity calibration because its $Z_{DR}(0)$ usually varies between 0 and 0.5 dB (Ryzhkov and Zrnic 1998 a, b). Furthermore, it can be identified within the cloud in regions slightly above the melting level. The melting layer can be detected by a sharp drop of the cross-correlation coefficient. Thus, in the regions of dry snow above the melting layer, the expected value of Z_{DR} near the 60° elevation angle should lie in the narrow range between 0 and 0.12 dB.

Fig. 5.4 presents an example of the RHI cross section recorded on 04/07/2002 at 14:41 UT. One can see low Z_{DR} above the melting layer that is located at about 2.5 km. Thus Z_{DR} calibration data should be taken above 2.5 km. Fig. 5.5 presents $Z_{DR}(60^o)$ recorded from 360° azimuth scans for three range (height) locations. Although $Z_{DR}(60^o)$ fluctuates over an interval of about 1 dB (most all of these fluctuations are due to statistical variations associated with small sample number estimates), the mean Z_{DR} (shown in the brackets in Fig. 5.5), obtained by averaging over azimuth, changes less than 0.04 over the heights from 4.7 to 6.3 km. During this data collection the system differential reflectivity offset, $Z_{DR\,OFF}$, was set at - 0.31 dB. Thus, using the average of the three means listed in Fig. 5.5, the true offset, calculated from these measurements, is about -0.34 dB. This is within a 0.1 dB of value -0.25 dB (see Eq.(5.22)) calculated from observations of drizzle.

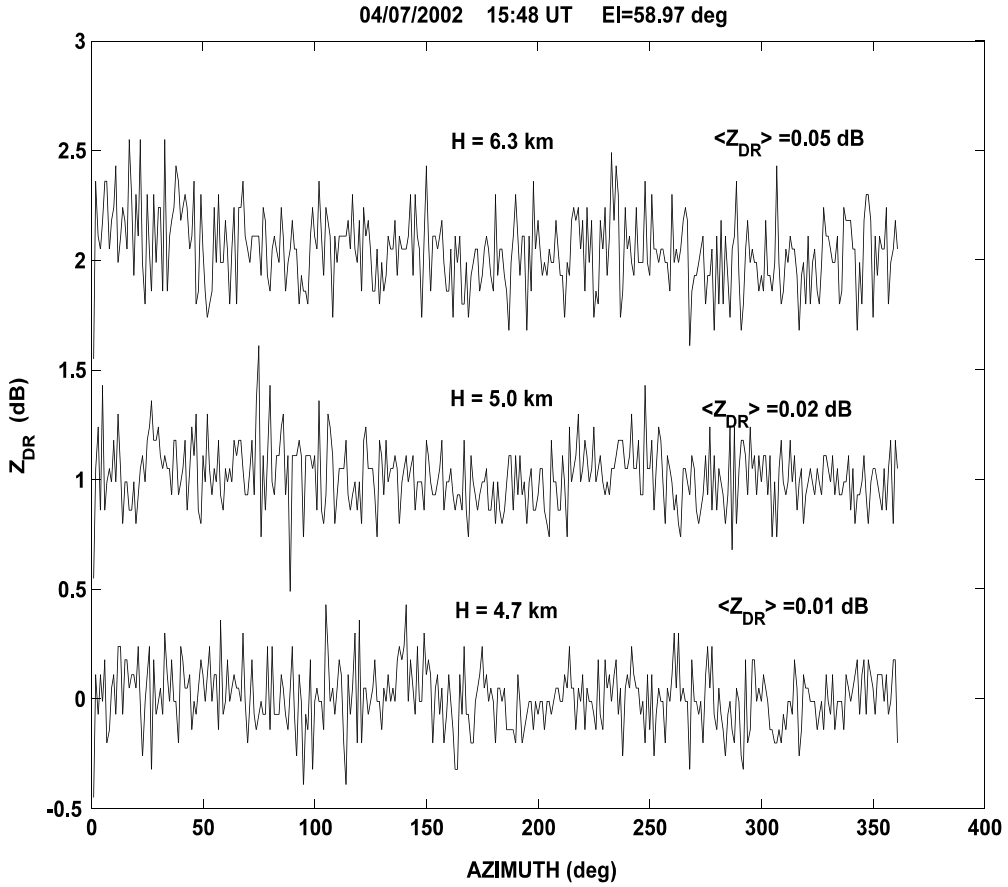

Fig. 5.5. Azimuthal dependence of Z_{DR}, for different heights at elevation of 60^0 for the cloud in Fig. 5.4. For visual clarity, the two upper curves are displaced by 1 dB from each other.

5.4 Z_{DR} calibration using the ground clutter

The Z_{DR} calibration using external scatterers such as precipitation is attractive because the overall calibration can be performed (i.e., this calibration measures the mismatches in both the transmitter as well as the receiver). But precipitation is not always present. Therefore we investigated the use of ground clutter as a means to calibrate Z_{DR} . Because the ground clutter has a highly variable Z_{DR} (e.g., Z_{DR} can exceed 10 dB) and can be positive or negative, the answer is no if data from a single range gate, arbitrarily selected, is used in the calibration. But a field of Z_{DR} from ground clutter offers attractive possibilities. We have been recording ground clutter data since May 2002. One full rotation of the antenna is used to collect data at low elevation. Only echoes with the SNR larger than 30 dB were processed so that the effects of noise are insignificant. An example of the output histogram of Z_{DR} is shown in Fig. 5.6.

The RVP7 processor presents the Z_{DR} values in the interval of -7.94 to 7.94 dB; all negative or positive values outside this interval are combined together as either -7.94 or 7.94 dB. Because ground clutter has some Z_{DR} values outside of this interval, the histogram has the long "horns" due to the finite interval of the Z_{DR} categories. The median, M, value of the histogram was calculated for the whole data set including the data within the "horns". M_2 is the median value for data only in the interval of -7 to 7 dB. The *Mean* value is also for the data in the interval -7 to 7 dB. In Fig. 5.7, these three values are shown over the time from May 2002 to November 2002. The averaged M is 0.07 dB with standard deviation of 0.23 dB, the averaged M_2 is 0.13 db with standard deviation of 0.14 dB, and averaged *Mean* is 0.07 dB with standard deviation of 0.11 dB. The Z_{DR} variations for the ground clutter could depend on many factors such as a stage of vegetation, the wind near the ground, wetness of vegetation, etc. We didn't sort our data into any such categories. Nevertheless, the measurements suggest that ground clutter is a candidate for Z_{DR} calibration. We are continuing the measurements to include the cold season so that seasonal statistics and long term variation of the Z_{DR} can be determined.

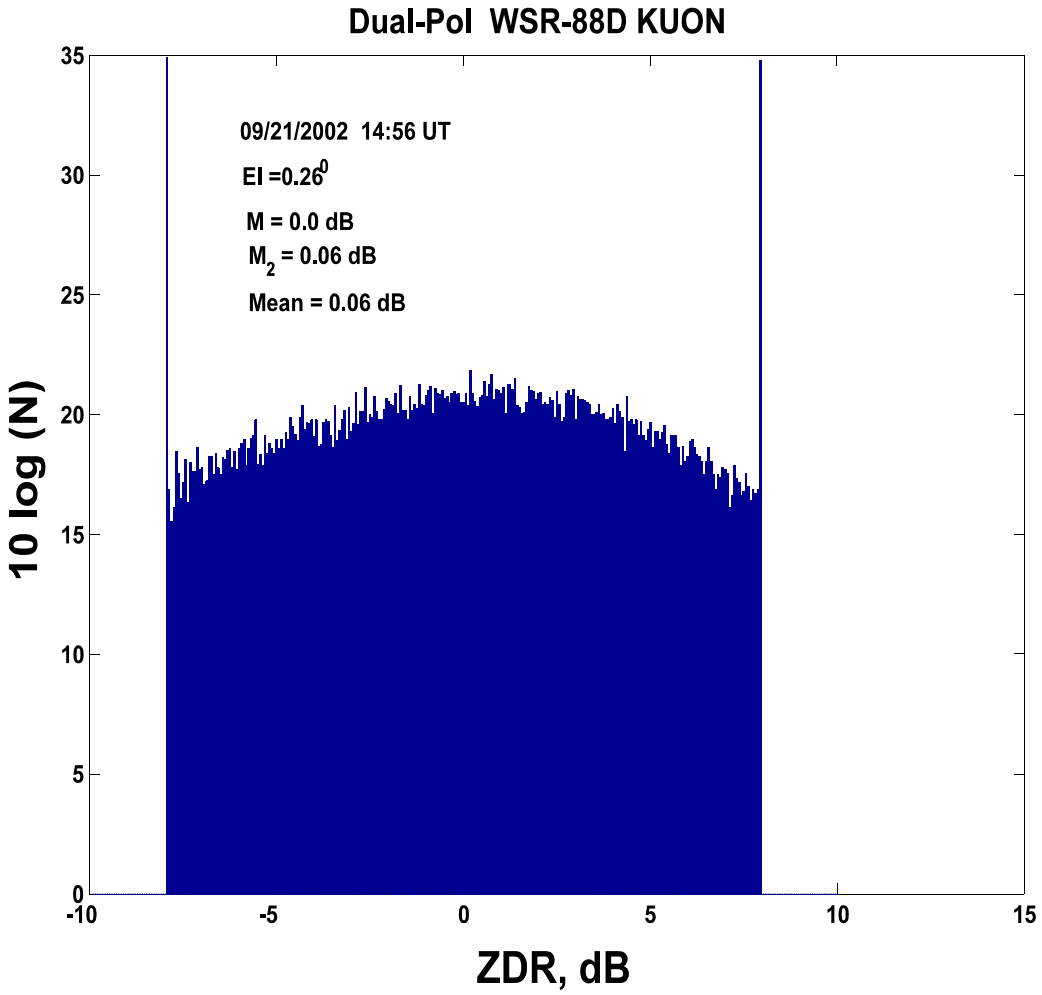

Fig. 5.6. Histogram of Z_{DR} from ground clutter for one full antenna revolution

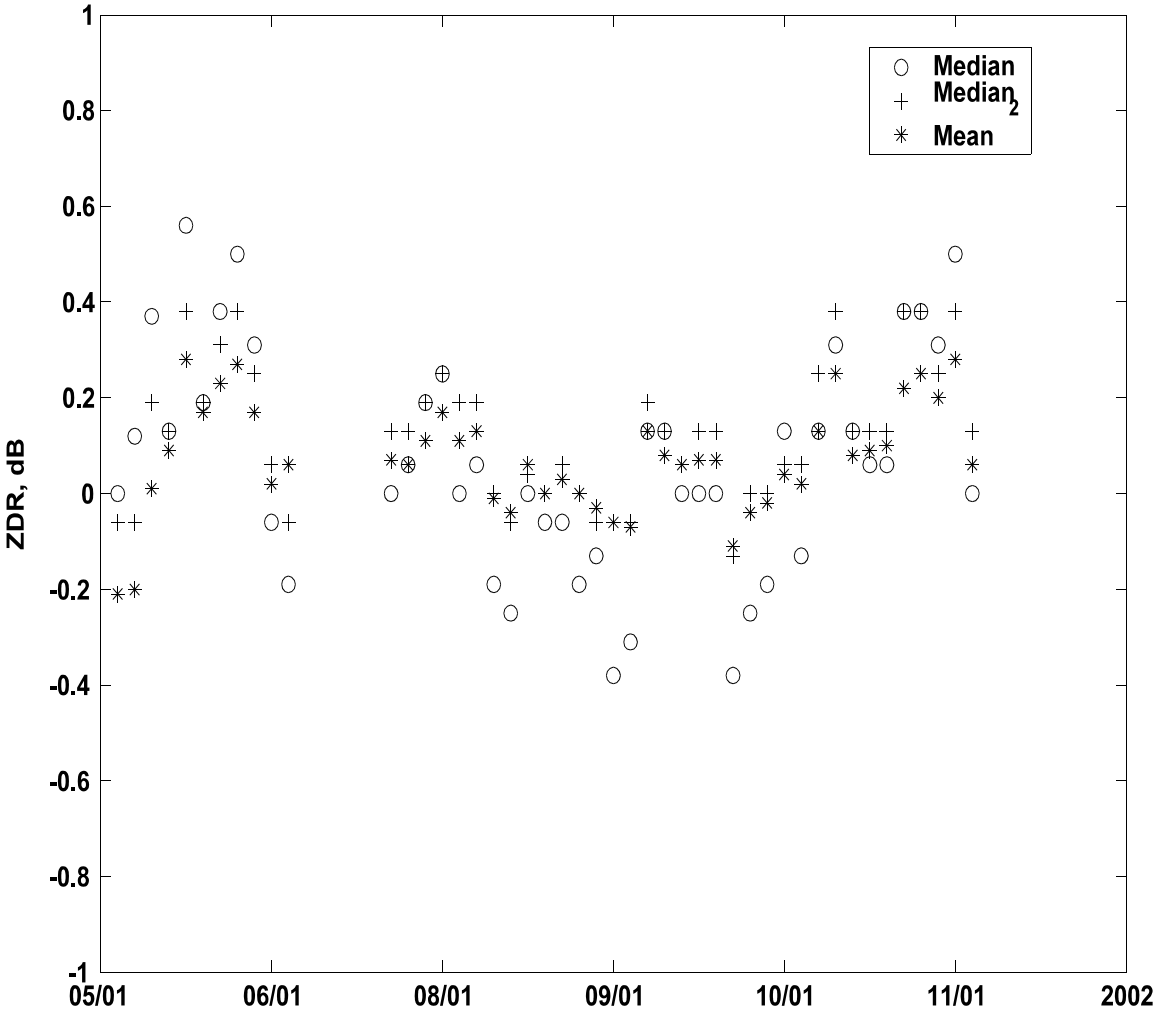

Fig. 5.7. Time variations of the Z_{DR} from the ground clutter.

6. Dual-Pol Reflectivity Calibration

SIGMET's RVP7 calibration procedure (RVP7 User's Manual, p. 5-13) uses the signal plus noise power P_h in horizontal channel, to compute Z_h. That is,

$$Z_h = 10\log\left(\frac{P_h - N_h}{N_h}\right) + \mathbf{dB}Z_{\mathbf{o}h} + 20\log\mathbf{r} + ar \qquad (6.1)$$

where dBZ_{oh} is a calibration reflectivity factor, r is the distance to a given resolution volume, and ar is the attenuation due to precipitation and atmospheric gases. Calibration measurements are usually performed in clear air at short ranges, and thus the attenuation factor ar can be ignored. The first term in Eq. (6.1) is the signal-to-noise-ratio. The accuracy of reflectivity calculations in the RVP7 is 0.5 dB.

NSSL's WSR-88D can operate in the two polarization modes: SHV and Depolarization. Radar calibration parameters are different in these modes so we consider these modes separately. In the next sections we will calculate dBZ_o.

6.1 Calibration of weather signal power in the SHV mode

The received weather signal plus noise powers at the output of the H and V receivers (Doviak and Zrnic, 1993, section 4.4.5)

$$P_h(\mathrm{mw}) = \frac{\pi^5 10^{-14} P_{th}(\mathrm{kW}) g_a^2 |K_w|^2 \tau(\mu s)\theta_1^2(\mathrm{deg}) Z_{eh}(\mathrm{mm^6 m^{-3}})}{6.75 x 2^{14} \ln 2 \ \lambda^2(\mathrm{cm}) \ r^2(\mathrm{km}) \ell_r} g_{\mathbf{h}} + N_h(\mathrm{mw}) \qquad (6.2a)$$

$$P_v(\mathrm{mw}) = \frac{\pi^5 10^{-14} P_{tv}(\mathrm{kW}) g_a^2 |K_w^2| \tau(\mu s)\theta_1^2(\mathrm{deg}) Z_{ev}(\mathrm{mm^6 m^{-3}})}{6.75 x 2^{14} \ln 2 \ \lambda^2(\mathrm{cm}) r^2(\mathrm{km}) \ell_r} g_v + N_v(\mathrm{mw}) \qquad (6.2b)$$

where the measurement units are identified in the brackets, and we assumed that the antenna gains, g_a, the one-way beamwidths θ_1, and the receiver's finite bandwidth loss factor l_r, are same for both polarization channels (Doviak et. al., 2002). Most of the paramters in Eq. (6.2) are fixed known values. For, example, $|K_w|^2 = 0.93$, and for matched filter receivers such as used in the WSR-88D, $\ell_r \approx 1.7$ (Doviak and Zrnic, 1993, Fig. 4.8). Furthermore, for the R&D WSR-88D radar, $\lambda = 11.1$ cm, $\theta_1 = 0.94^o$, $\tau = 1.57$ μs (for the storm mode of data collection), and $g_a = 2.82 \times 10^4$ (i.e., $G_a = 44.2$ dB). Substituting these values into Eqs. (6.2) and solving for Z_e,

$$Z_{eh}(mm^6m^{-3}) = \frac{5.21\ 10^9 r^2(km)[P_h(mW) - N_h(mW)]}{P_{th}(kW)g_h} \quad , \tag{6.3a}$$

$$Z_{ev}(mm^6m^{-3}) = \frac{5.21\ 10^9 r^2(km)[P_v(mW) - N_v(mW)]}{P_{tv}(kW)g_v} \quad . \tag{6.3b}$$

The RVP7 uses a calibration reference reflectivity factor Z_o which is the one that gives a signal power equal to the noise power at a range of 1 km with the measured transmitted powers. Using those values P_{th} = 160 kW and P_{tv} = 164 kW stated in section 5.1.2 and expressing the reflectivity factor in decibel units, the reference reflectivity factors are

$$Z_{0h}(\text{dBZ}) = 75.13 - G_h(\text{dB}) + N_h(\text{dBm}) \ , \tag{6.4a}$$

$$Z_{0v}(\text{dBZ}) = 75.02 - G_v(\text{dB}) + N_v(\text{dBm}) \ , \tag{6.4b}$$

The last terms in Eqs. (6.4) are the noise powers, expressed in dBm units, at the outputs of the receivers. Note that because the output noise power, in decibel units, is $G + N^{(i)}$, Eqs. (6.4) can be expressed in terms of the input noise power as

$$Z_{0h} = 75.13 + N_h^{(i)}(dBm) \ , \tag{6.5a}$$

$$Z_{0v} = 75.02 + N_v^{(i)}(dBm) \ , \tag{6.5b}$$

Thus the reference reflectivity factors are independent of the gains if the input noise powers do not change. Although changes in amplifier gains after the LNAs should not significantly change the input noise power, changes in the LNA gains do. This is because most of the noise power originates in the LNAs, and changes in LNA gains could significantly change $N^{(i)}$ (i.e., noise power referenced to the antenna port) and thus will change Z_o. The mean input noise powers, calculated in section 9, are: $N_h^{(i)}$ = -109 dBm; and $N_v^{(i)}$ = -110 dBm. Substituting theses values into Eqs. (6.5) gives

$$Z_{oh} = -33.9 \text{ dB}Z \ , \qquad Z_{ov} = -35.0 \text{ dB} \ . \tag{6.6}$$

These values should be downloaded into the RVP7.

The values in Eq. (6.6) are for the reference distance of 1 km. For the distance of 50 km these values become 0.1 dBZ and -1.0 dBZ. The legacy WSR-88D has a specified performance is that the a reflectivity factor of -7.5 dBZ at 50 km should produce a signal power equal to or larger than the noise power (Doviak and Zrnic 1993, Table 3.1). The difference between the legacy performance and that calculated for the polarimetric upgraded R&D WSR-88D, operated in the SHV mode, is due to the following reasons: 1) reduced transmitted power in each of the linearly

polarized waves, 2) the increase in input noise power, and 3) the increase of attenuation caused by additional polarization hardware.

The legacy WSR-88D transmits 475 kW whereas the polarimetric WSR-88D transmits about 160 kW; this accounts for an increase loss in performance of about 4.7 dB. The legacy WSR-88D has a specified noise power, referenced to the antenna port, of -113 dBm; this accounts for an additional 4 dB loss in the H channel performance, and an additional 5 dB loss for the V channel performance. Some of the increased noise is due to the larger bandwidth used with the polarimetric WSR-88D. Also, additional hardware has been added between the LNAs and the antenna port which increases the losses and hence the noise power referenced to the antenna port. Finally, there could be an additional increase of noise power due to changes in the performance of the LNAs. Note that the noise bandwidth of H channel of the polarimetric WSR-88D is larger than that for the V channel and that accounts for the larger noise power for the H channel versus that for the V channel. Comparing with -7.5 dBZ for the legacy system, we find a difference of about 2.1 dB for the horizontal channel and 1.1 dB for the vertical channel.

6.2 Calibration of weather signal power in the Depolarization mode

For radar calibration in the Depolarization mode (DM), we can use Eq. (6.3a), and substitute the power transmitted in the mode. The value of transmitted power (i.e., P_t (DM) = 323 kW) reported by Doviak et al. (2002, p.7) is representative of the transmitted power at the antenna port. The input noise power in the DM is equal to the input noise power in the H channel for the SHV mode of operation; that is N_h (DM) = -109 dBm. Thus the reference reflectivity factor for the DM is

$$Z_{oh}\,(\mathrm{DM}) = -36.9\ \mathrm{dB}Z \tag{6.7}$$

This value should be downloaded into the RVP7 processor.

For the reference distance of 50 km this value becomes -2.9 dBZ. If the RVP7 is connected to output J3 of the V channel mixer-pre-amplifier (Fig. 3.1), the reference reflectivity factor Z_o would be 5 dB less (i.e., Z_{ov} = -7.9 dBZ). Comparing with the - 7.5 dBZ for the legacy system, we find about a 0.4 dB difference.

7. Calibration of copolar and cross-polar parameters

7.1 Propagation phase shifts

The outgoing waves in the two channels, $E_h^{(T)}$ and $E_v^{(T)}$, can be represented as:

$$E_h^{(T)} = (g_a^{1/2} P_0 / l_h)^{1/2} \exp[-j\omega t],$$
$$E_v^{(T)} = (g_a^{1/2} P_0 / l_v)^{1/2} \exp[-j\omega t + j\Phi^{(T)}] \quad (7.1)$$

where g_a is the antenna power gain, ω is the career frequency, t is time, and $\Phi^{(T)}$ is the system differential phase in transmit. We assume that the antenna gain for horizontally and vertically polarized waves is the same; this is a good assumption and has been demonstrated by measurements (Doviak, et. al., 2000).

The horizontal and vertical scattered waves at the antenna horn are expressed as:

$$E_h^{(A)} = \frac{C^{1/2}}{R\, l_h^{1/2}} \eta_h^{1/2} \exp[-j\omega t + j\varphi_{dp}] \quad (7.2a)$$

$$E_v^{(A)} = \frac{C^{1/2}}{R\, l_v^{1/2}} \eta_v^{1/2} \exp[-j\omega t + j\Phi^{(T)}] \quad (7.2b)$$

where,

$$C = \frac{P_0 \lambda^2 c \tau \pi \theta^2 g_a^2}{(4\pi)^3 16 \ln 2} \quad (7.2c)$$

where η_h and η_v are reflectivities for horizontal and vertical waves (as stated earlier, for precipitation we can neglect cross polar components), C is the radar constant, λ is the wavelength, c is the speed of light, τ is the radar pulse duration, θ is the antenna beamwidth. Derivation of the radar constant can be found in (Doviak, Zrnic; 1993).

We need additional three parameters to characterize the system. These are receiver gain in the horizontal channel, $g_h^{(R)}$, receiver gain in the vertical channel, $g_v^{(R)}$, and the phase difference between horizontal and vertical signals, $\Phi^{(R)}$. Equations (7.2) express the voltages at the antenna horn, the corresponding voltages at the input to the IF digitizer can be written as:

$$V_h = \frac{C^{1/2}}{R\, l_h^{1/2}} g_h^{(R)1/2} \eta_h^{1/2} \exp[-j\omega_{IF} t + j\varphi_{dp}] \tag{7.3a}$$

$$V_v = \frac{C^{1/2}}{R\, l_v^{1/2}} g_v^{(R)1/2} \eta_v^{1/2} \exp[-j\omega_{IF} t + j\Phi^{(T)} + j\Phi^{(R)}] \tag{7.3b}$$

$$\Phi_{SYS\ SHV} = \Phi^{(T)} + \Phi^{(R)}, \tag{7.3c}$$

where $\omega_{\rm IF}$ is the intermediate frequency including the Doppler shift and $\Phi_{\rm SYS\ SHV}$ is the system differential phase in the SHV mode.

Using Eq. (7.3), we obtain for the polarimetric variables in the SHV mode:

$$P_h = \frac{C}{R^2 l_h} g_h^{(R)} \eta_h \tag{7.4a}$$

$$P_v = \frac{C}{R^2 l_v} g_v^{(R)} \eta_v \tag{7.4b}$$

$$\rho_{hv} = |\rho_{hv}| \exp[j(\varphi_{dp} - \Phi^{(T)} - \Phi^{(R)})]. \tag{7.5}$$

Equations (7.4) express the powers of the weather signals received by a radar. The two receivers have different noise powers. Assuming that the system is linear for weak signals, we can express the two noise powers as

$$N_n = g_h^{(R)} N_{th}^{(i)}, \qquad N_v = g_v^{(R)} N_{tv}^{(i)},$$

where $N_{\rm th}$ and $N_{\rm tv}$ are total noise powers resulting from atmospheric and system noise referenced to the antenna horn. The atmospheric noise is the same for the two channels, but system noise is different because the horizontal and vertical channels consist of physically different hardware.

7.2 The copolar correlation coefficient

The complex copolar correlation coefficient, ρ_{hv}, between voltages in the H and V channels is,

$$\rho_{hv} = \frac{1}{M}\sum_{m=1}^{M} V_{hh}(m)V_{vv}^{*}(m) / \sqrt{(P_{hh} - N_h)(P_{vv} - N_v)} \tag{7.6}$$

The differential phase, φ_{dp}, is the argument of ρ_{hv} , and is the difference between the phases of the H and V signals. That is,

$$\varphi_{dp} = \arg\left(\frac{1}{M}\sum_{m=1}^{M} V_{hh}(m)V_{vv}^{*}(m) \right) \tag{7.7}$$

For echoes from precipitation, φ_{dp} increases with range.

In the SHV mode, the RVP7 calculates the differential phase using (4.6) with an offset $\varphi_{\mathrm{dp\,OFF}}$:

$$\varphi_{dp} = \arg\left(\frac{1}{M}\sum_{m=1}^{M} V_{hm}V_{vm}^{*} \right) + \varphi_{dp\ OFF}, \tag{7.8a}$$

$$\varphi_{dp\ OFF} = -\Phi_{SYS\ SHV}. \tag{7.8b}$$

Like in the case of differential reflectivity, the $\varphi_{\mathrm{d\,p\,OFF}}$ is to compensate for the system differential phase $\Phi_{\mathrm{SYS\,SHV}}$ which is caused by radar hardware. The system differential phase has substantially lower influence on the polarimetric measurements than the $Z_{\mathrm{DR\,SYS}}$ because usually the derivative of the differential phases (so called K_{dp}) is of interest. But correct setting of this offset is important. The RVP7 has a 180° unambiguous interval for differential phase measurements. The total possible φ_{dp} interval is 360°, but the Sigmet uses the interval 180° to obtain a better phase resolution for 1 byte data representation. That is why the measured differential phase should start with values close to zero to preserve the maximal 180° interval and the $\varphi_{\mathrm{d\,p\,OFF}}$ should be close to the negative $\Phi_{\mathrm{SYS\,SHV}}$. The $\varphi_{\mathrm{dp\,OFF}}$ is set up as a parameter for the processing software of the RVP7.

7.3 The cross-polar correlation coefficient

In the Depolarization mode, the system measures the powers in the H and V channels and calculates the linear depolarization ratio, L_{DR}, as

$$L_{DR} = 10\log\left(\frac{P_{vh} - N_v}{P_{hh} - N_h}\right) \tag{7.9}$$

In the Depolarization mode, the complex coefficient ρ_h of the cross-polar correlation between the cross-polar voltage V_{vh} and the copolar voltage V_{hh}^* are calculated using Eq. (7.6) in which the copolar voltages V_{hh} and V_{vv}^* are replaced with the cross-polar and copolar voltages. The differential phase φ_{dp} (DM) in this mode is the argument of ρ_h. The correlation coefficients ρ_{hv} and ρ_h depend upon the forward and back scattering characteristics of the hydrometeors. If the differential phases upon back scatter can be neglected, the differential phase measured in the SHV mode is two times the value measured in the Depolarization mode.

8. Calibration of L_{DR}

In the Depolarization mode, the system uses the same offset for the differential phase and an $L_{DR\,OFF}$ offset for the L_{DR} measurements:

$$L_{DR} = 10\log\left(\frac{P_v}{P_h}\right) + L_{DR\,OFF} \tag{8.1}$$

Again, Eq. (8.1) is written without noise corrections and we have to compensate for noise outside the RVP7. The $L_{DR\,OFF}$ is to compensate for the system linear depolarization ratio, $L_{DR\,SYS}$, and is set up as a parameter for the processing software of the RVP7.

One can see from Eq. (7.6) that differential system gain doesn't affect the measurements of the correlation coefficient if noise is negligible. The measured differential phase, $\varphi_{dp\,(m)}$, with the RVP7 is

$$\varphi_{dp\,(m)} = \frac{1}{2}\varphi_{dp} - \Phi^{(R)} + \varphi_{dp\,OFF}\,, \tag{8.2}$$

The $\varphi_{dp\,OFF}$ should compensate for the differential phase in-receive

$$\varphi_{dp\;\;OFF} = -\Phi^{(R)}\,. \tag{8.3a}$$

$$\Phi_{SYS\ DM} = \Phi^{(R)} \qquad (8.3b).$$

In the Depolarizartion mode, we have to introduce different transmit loss, l_{DM} , because the transmit path differs from the transmit path in the SHV mode (see Fig. 1.1). For the power at the antenna horn, $P_{\mathrm{h}}^{(\mathrm{T\ DM})}$, we write

$$P_h^{(T\ DM)} = P_0 / l_{DM} \quad . \qquad (8.4)$$

For the RVP7, the measured linear depolarization ratio can be expressed as (see Eq. (5.4) for comparison with the SHV mode):

$$L_{DR\ (m)} = 10\log\left(g_v^{(R)} l_{DM}\, \eta_{hv}\right) + L_{DR\ OFF} = L_{DR\ SYS} + L_{DR} + L_{DR\ OFF} \ . \qquad (8.5)$$

$$L_{DR\ SYS} = 10\log(g_v^{(R)} l_{DM}) \ . \qquad (8.6)$$

From (8.6) we see that the $\mathrm{L_{DR\ OFF}}$ offset should compensate for the system offset:

$$L_{DR\ OFF} = -L_{DR\ SYS} \ . \qquad (8.7)$$

We see that the offsets for differential phase measurements in the SHV and DM modes are different. The RVP7 uses the same phase offset in the SHV and DM modes and this is not appropriate. This doesn't affect the meteorological parameters because they depend on the difference of the differential phases. Because the interval of phase measurements is 180º, the phase offsets should be set very close to negative system differential phases $\Phi^{(\mathrm{T})} + \Phi^{(\mathrm{R})}$ in the SHV mode and $\Phi^{(\mathrm{R})}$ in the Depolarization mode.

9. Measurements of the system differential phases

As it was shown in sections 7.1 and 8, the system differential phases in the SHV and Depolarization modes are different. These phases can be determined using the radar signal reflected from weather echo edges closest to a radar. Neglecting the phase shift upon scattering, the phase difference between H and V waves is equal to the system differential phase. Fig. 9.1 illustrates this for the SHV mode. To estimate the $\Phi_{\mathrm{SYS\ SHV,}}$ one should measure differential phases at the cloud edge nearest to a radar. Such values are shown in Fig. 9.1 with crosses. The mean for the crosses is 42.8^0 and this is an estimation of the system differential phase in the SHV mode. The standard deviation of the estimate is 5.1^0 with maximum deviation of 22^0. In accordance with the $\Phi_{\mathrm{SYS\ SHV}}$ definition (7.3c) we have for the system differential phase in this mode

$$\Phi_{\mathrm{SYS\ SHV}} = 42.8^0. \qquad (9.1)$$

The system differential phase can be also measured using a radar return from a strong point target under fear weather conditions. A radio tower can be used as such an object. A tower has its own differential phase and our radar observations show that this phase is quite different for different towers. But the differential phase for a given tower is very stable over time and can be used to monitor the drift of the system differential phase. In the vicinity of our radar, there are several radio towers that reflect strong signal so that the signal-to-noise ratios are very high. Among those towers we found a tower with the intrinsic differential phase close to the differential phase (9.1). An example of the φ_{dp} for the radio tower situated at Az= 306.12^0 and the distance of 28.939 km is shown in Fig. 9.1 with a line. The measured mean differential phase of 43.2^0 is very stable; the standard deviation is of 1.2^0 for the period of 7 minutes. The mean measured differential phase is persistent; daily variations are in the limits of $\pm 7^0$. So we can use the tower measurements to monitor the system differential phase.

In the Depolarization mode, it is hard to use weather objects for the estimation of the system differential phase because cross polarized signal is usually weak and reflections from closest cloud edges can not be used like in the SHV mode. But strong radar returns from a tower can be used for that. An example of the measurements is shown in Fig. 9.2. The depolarized signal is strong and the measured differential phase is 52.0^0 with the standard deviation of 3.2^0. Comparison with the cloud differential phase in the Depolarization mode show that the phases for the tower is approximately 33^0 higher than for clouds due to intrinsic phase of the tower. So in the Dopalarization mode, the estimation of the system differential phase is

$$\Phi_{SYS\ DM} \approx 52.0^0 - 33^0 = 19^0. \qquad (9.2)$$

Using Eqs. (7.3c) and (8.3b) and the measured system phases (9.1) and (9.2) the system differential phases on-receive and on-transmit can be obtained:

$$\Phi^{(R)} = 19^0, \quad \Phi^{(T)} = 23.8^0. \qquad (9.3)$$

The tower radar measurements can be used to set up the system phase differential offsets and to monitor the system phase drifts.

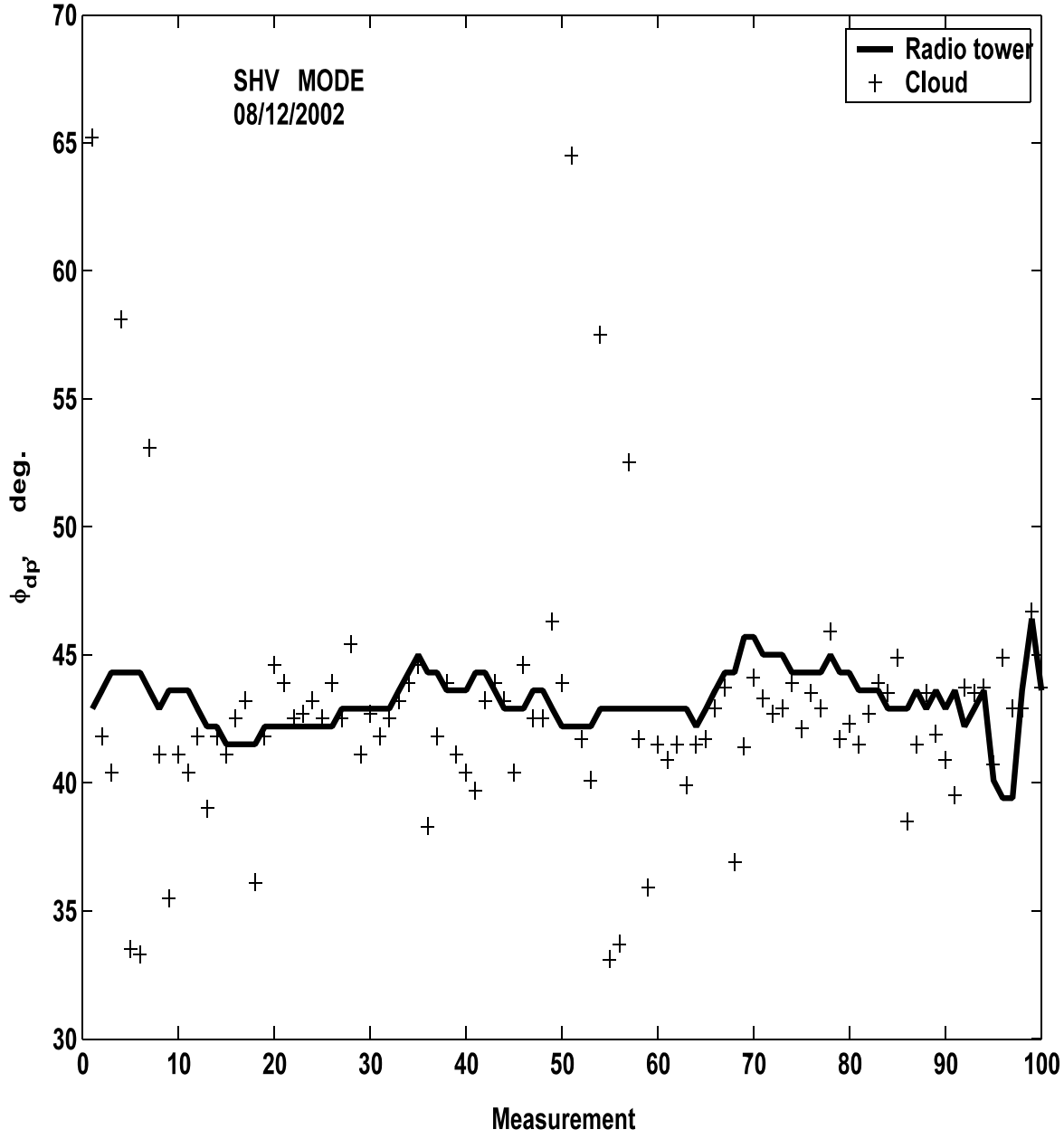

Fig. 9.1. The differential phases measured at the cloud edge nearest to the radar on 08/12/2002 1347 UT (crosses) and from the radio tower at 1515 UT (line). SHV mode. Measurements are numbered sequentially.

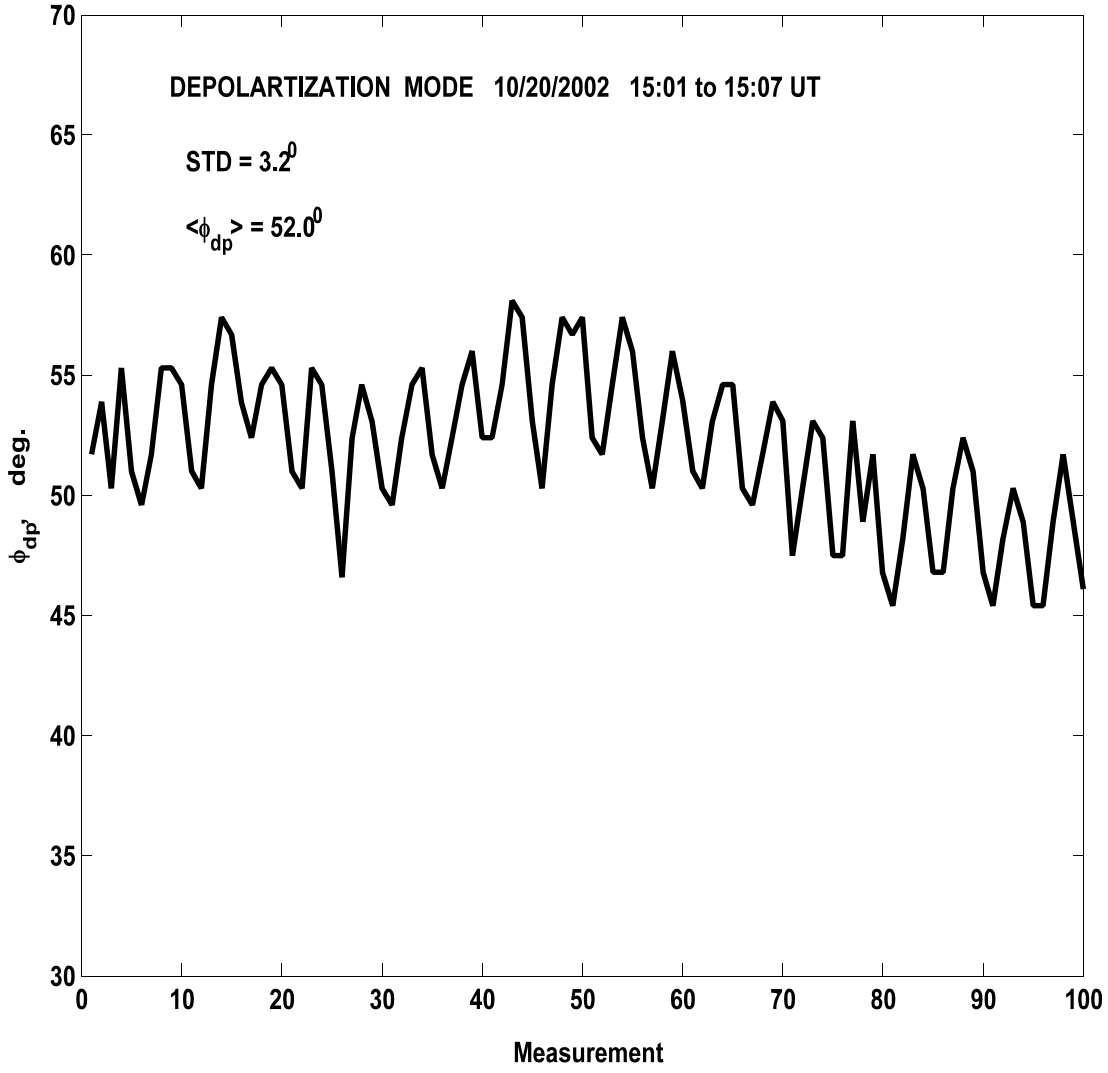

Fig. 9.2. Differential phases of signal from the radio tower. Depolarization mode.

10. System noise measurements

Precise noise measurements are very important in polarimetric radar observations. For a given reflectivity, the signal-to-noise ratio decreases with range, and therefore the noise corrections become more important with range. In a cloud, noise influence increases with the height because generally reflectivity decreases with height so that even for sufficiently short distances the noise corrections need to be applied at high elevations.

The need for noise corrections depends on the signal-to-noise ratio, SNR, which in turn depends on the input noise power $N^{(i)}$. $N^{(i)}$ establishes the minimal weather signal power level at the antenna port that equals the noise power. In turn, this establishes the minimum reflectivity needed to make credible estimates of Doppler moments and polarimetric parameters. To measure $N^{(i)}$ an external CW RF generator was connected to the calibration port 8. The 3 dB method was used in making these measurements.

10.1 System noise of the legacy WSR-88D

To measure $N^{(i)}$ of the legacy system, the receive legacy circuitry was used (see port J3 at the H mixer-preamplifier in Fig. 3.1). The 3-dB method has been applied while the system was in the 'Standby' stage. The output power was measured using the system readings of the output power expressed in the PSP units (PSP stands for Programmable Signal Processor in the legacy WSR-88D). The antenna was in the park position. The results of the measurements on 11/01/2002 are as follows:

Lin. Channel Noise (short pulse) = 0.191 10^{-5} PSP units
+3 dB signal = 0.383 10^{-5} PSP units
Generator's power (3 dB signal) P_{gen} = -83.7 dBm
Cable attenuation L_c = 8.66 dB
Waveguide Coupler's attenuation L_{wc} = 21.3 dB
Attenuation between the antenna port and the waveguide coupler L_{wca} = 0.65 dB

The L_c was measured**,** the losses L_{wc} and L_{wca} were taken from the radar adaptation file.[4] Using the above parameters, we get the input noise power for the H channel, (i.e., $N_h^{(i)}$) when the radar is operated with short transmitted pulses (i.e., the storm mode):

[4]When the polarimetric upgrades were added to the R&D WSR-88D, the only change in the H channel receiver was a new azimuthal rotary joint, and additional waveguides between the H circulator and the azimuthal rotary joint. The insertion loss of the new rotary joint is less than 0.1 dB, about that of the one that it replaced. Waveguides, including a flexible guide and several bends, were added between the circulator (the circulator was moved outside the pedestal) and the rotary joint in order to facilitate installation of the polarimetric upgrades. But the added waveguides should not have increased the losses by more than a tenth of a dB.

$$N_h^{(i)} = P_{\text{gen}} - L_{\text{c}} - L_{\text{wc}} + L_{\text{wca}} = -83.7 - 8.66 - 21.3 + 0.65 = -113.0 \text{ dBm} \quad (10.1)$$

Assuming the root mean square (i.e., rms) uncertainties of each measurements is ±0.1 dB, the legacy's $N_h^{(i)}$ is -113.0 ± 0.2 dBm. It is comforting that $N_h^{(i)}$ is exactly the same as that specified in the Table 3.1 of Doviak and Zrnic (1993). Note that the specified values are not necessarily those that were measured on the legacy radar before the polarimetric upgrades, but are performance specifications that should be met by the WSR-88D if the radar's parameters (e.g., LNA noise figure, transmitted powers, etc.) are nominal.

10.2 System noise of NSSL's polarimetric WSR-88D

Using the 3-dB method, we measured the input noise power for the two polarization channels. The output powers were recorded with the RVP7 signal processor. The RVP7 can be connected to the two outputs from the mixer-preamplifier (Fig. 3.1); that is, to either the J3 output which is usually used by the legacy circuitry, or to the J4 output which has a signal plus noise power level 17 dB below the power level at the output at J3. The results of the measurements on 11/01/2002 are presented in Table 10.1. The noise levels of each of the channels were calculated using Eq. (10.1). The RVP7's bandwidth was tuned up to the short radar pulse (1.57 μs). One can see from the table that there is a 3 dB noise powers difference if the measurements are made at the J3 or J4 connections. To understand the difference one should consider noise internal to the RVP7.

A power measurement device (i.e., the RVP7) has its own internal noise which can be referred to the input to the antenna port. If N_{r} and N_m are the noise levels of a receiver and a measurement device referred to the antenna port, then the noise level at this port is

$$N^{(i)} = 10\log (N_{\text{r}} + N_m). \quad (10.2)$$

We see that $N^{(i)}$ will be determined by the receiver and atmospheric noise if $N_{\text{r}} >> N_m$. The internal RVP7 noise can be measured by terminating its input. With the input to the RVP7 terminated with a matched impedance load (i.e., a 50 ohm termination), the noise powers measured at the RVP7 input are -80.27 dBm in horizontal channel and -79.95 dBm in vertical channel. Noise powers measured at the input to the RVP7 (i.e., this would be the output of the H and V analog channels of the WSR-88D; Fig. 3.1) when the radar's analog dual IF receiver outputs are connected to the RVP7 are shown in Table 10.1 (i.e., first row). For the vertical channel we have $N_m = 1\ 10^{-8}$ mW, and $N_r = 68.9\ 10^{-8}$ mW when the RVP7 is connected to the J3 output. We see the first value is about 18 dB larger than the second one so that $N_{\text{r}} >> N_m$ and the noise power referred to the antenna port is determined by the LNA and associated waveguide components and not the RVP7.

But when the RVP7 was connected to the J4 output, the measured analog receiver output noise power was $N_r = 3.2\ 10^{-8}$ dBm, and thus only about 5 dB larger than N_m . Under these conditions, the internal noise power of the RVP7 cannot be ignored. In order to prevent the performance from deterioration by the internal noise of the RVP7, we need to add more IF gain to the analog receivers.

Table 10.1. Noise levels of the H and V channels

	Horizontal Channel	Vertical Channel	
	J4	J3	J4
Noise Power, dBm	-73.9	-61.62	-75
+3 dB signal, dBm	-79.9	-84	-81
Loss, L_c , dB	8.66	8.66	8.66
Loss, L_{wc} , dB	21.3	21.3	21.3
Loss, L_{wca} , dB	0.65	0.65	0.65
MDS , dBm	-109.2	-113.3	-110.3

The input noise power of the vertical channel is about 1 dB less than that for the horizontal channel. As it was shown in section 3, the increased noise power in the H channel is due to the larger noise bandwidth of the H channel. The noise bandwidth in the H-channel is 1.3 times larger than the noise bandwidth of the V channel, and thus the noise power in the H channel should be 1.1 dB larger; this is in agreement with values listed in Table 10.1. Further proof was obtained with the following measurements.

Using the WSR-88D's built-in RF noise generator, the Z_{DR} was measured for normal connection at points 4 and 5 in Fig. 3.1 and then for flipped connection: i.e., the output from the LNA in the horizontal channel was connected to the directional coupler in the vertical channel and the output from the LNA in vertical channel was connected to the directional coupler in the horizontal channel. The polarimetric parameters were measured with the RVP7. The results of the measurements are in Table 10.2

Table 10.2. Measured polarization parameters for the two signal paths

	Normal Connection	Flipped Connection
Built-in attenuator, dB	0	0
Horiz. Reflectivity, dB	20.5	20.5
Z_{DR}, dB	2.03	2.03
φ_{dp}, ^{o}	53	133
ρ_{hv}	0.88	0.88

We see the differences in differential phase only. The mean noise Z_{DR} is about 1.1 dB. The lower bound depends on current noise levels in the channels and varies in the interval of 0.88 to 1.3 dB over time.

10.3 Time stability of system noise

The noise levels in the channels were measured during the sun scans while the antenna was pointed to the blue sky at elevations more than 15^{o}. The measurement period contains May to June and August to December 2002. Fig. 10.1 presents the corresponding results. One can see that the variations of the input noise power in two channels are mostly within ±0.5 dB. To account for noise in polarization measurements, the system has to measure the noise levels after each VCP. That is, the polarimetric WSR-88D should measure noise levels the same way as it is done in the legacy system and as often as the legacy system makes these measurements.

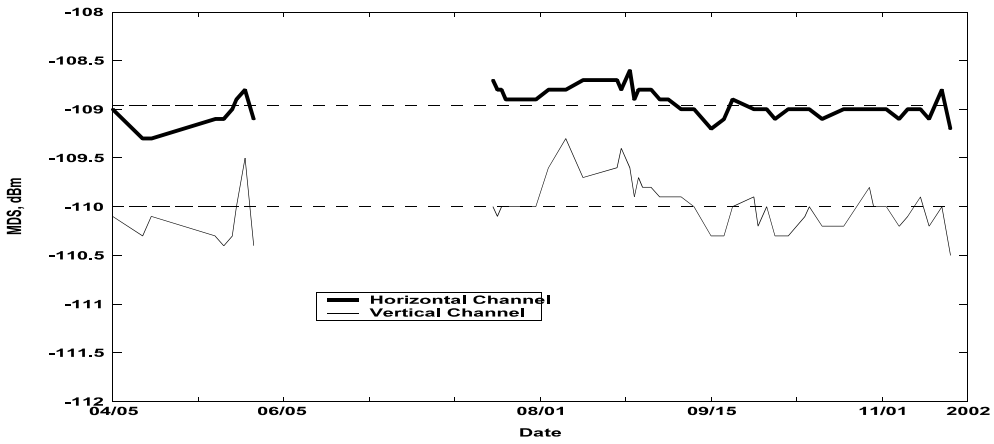

Fig. 10.1. Time variations of the minimal detectable signal (MDS) in the H and V channels.

11. Two channel dynamic range measurements

To measure the dynamic range of the system, we used a scheme presented by a block diagram in Fig. 3.1 with an external CW RF generator connected to port 8, and a spectrum analyzer connected to the output from the mixer-preamplifier at J3. An HP 8648C has been used as a RF generator and the spectrum analyzer was the HP 8563A. The results of the measurements are shown in Fig. 11.1. The curves for horizontal and vertical channels coincide within an accuracy of 0.5 dB. There are deviations of about 1 dB in the region near -80 dBm of the generator power. The slope of the curves was calculated in the interval of -60 to 0 dBm and it is 1.03. The dotted line in the figure represents the difference between the power the receiver would have if the response is determined by the mean slope, versus the actual power in the vertical channel measured by the spectrum analyzer. At the upper part of the dynamic range, the compression point of 1 dB was chosen to calculate the upper limit of linear dynamic range. It corresponds to + 9 dBm of the generator power. At the other end the receiver noise limits the performance of the radar at -75 dBm. Often the 1 dB detection threshold is used to determine the low bound of the dynamic range. The 1 dB detection threshold is taken to be 1 dB above the noise level as shown in Fig. 11.1. For the R&D WSR-88D, this is at -85 dBm of the generator power. So the dynamic range of the receivers is +9 - (-85) = 93 dB.

The 1 dB detection threshold doesn't establish the 'low signal' limit of the dynamic range. We can apply a simple scheme of linearization for weak signals: we can subtract the noise power from the measured signal+noise power. Fig 11.2 presents the results of the linearization for the vertical channel. The noise power and signal+noise powers were estimated using 256 samples in 100 range bins (i.e., a total of 25600 samples). The procedure shows linearity of the channel down to -101 dBm of generator's power so that we can add 16 dB more to the 93 dB 'classical' dynamic range. The total dynamic range of the receivers is then 109 dB. The purity of the dynamic range curve under the noise level means absence of unwanted signals like leakage from other devises or contamination with the 60-Hz power sources. It shows the very high quality of the system.

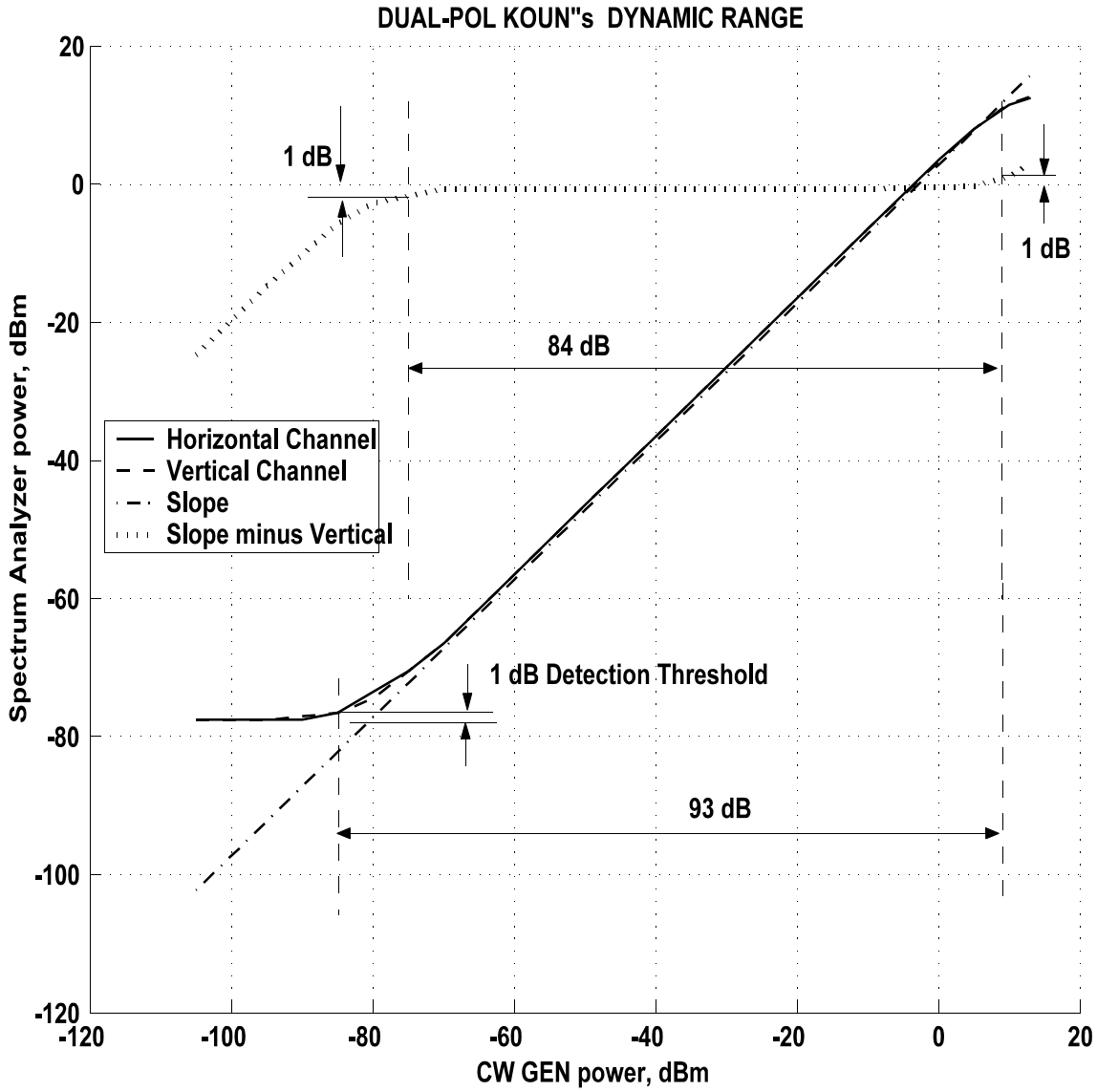

Fig. 11.1. Dynamic range of the dual-pol receivers.

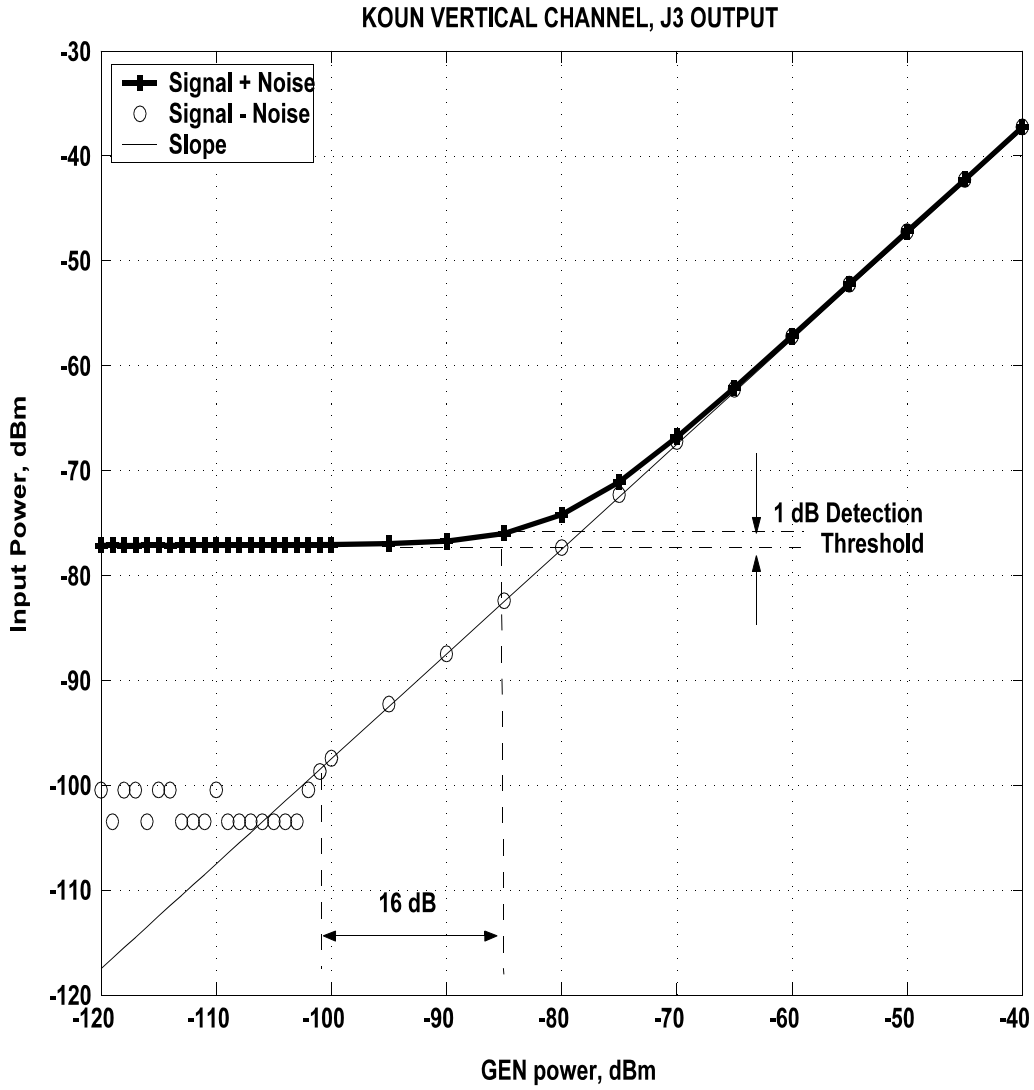

Fig. 11.2. Receiver characteristic at weak signals for the V channel.

12. H and V beam alignment

The data collected during sun scans can also be used to verify the coincidence of the H and V beam axes. To check the alignment of the radar beams (for the H and V polarizations), the antenna beam scanned through the solar disk in azimuth at a constant elevation angle. An example of the results of the measurements is presented in Fig. 12.1. This figure is a central part of Fig. 5.1 but presented with a finer resolution. We see from the figure that signal maxima coincide in H and V channels. This means that possible misalignment of the beam in the azimuthal direction is less than the accuracy of azimuthal resolution (i.e., $< 0.05^o$). To check the alignment in the vertical direction, the antenna beam was made to scan through the solar disk in elevation at a constant azimuth angle. An example of the data is shown in Fig. 12.2. The vertical dash lines in Figs. 12.1 and 12.2 are drawn at the maximums in H channel. One can see that the positions of signal maxima coincide, and hence we conclude that alignment in azimuth and elevation is satisfactory and possible misalignment is less than 0.05^o.

13. Effects of the rotary joints on the polarization measurements

In the NOAA's polarimetric WSR-88D, the one-channel azimuthal rotary joint has been changed on a two-channel azimuthal rotary joint and the elevation rotary joint has been mounted in the V-channel (see Fig. 3.1). The azimuthal and elevation rotary joints can contribute to the system $Z_{DR\,SYS}$ and φ_{dp} offsets. If the differential losses of the rotary joints depend upon angle, there will be an angular dependence of the $Z_{DR\,SYS}$ and $\Phi_{SYS\,SHV}$. To check this out, the following measurements have been made. The external CW RF generator HP 8648C was connected to ports 6 and 7 using a coax power splitter so that the generator fed the ports simultaneously. The KOUN's antenna was moved over azimuth with fixed elevations and then over elevation with fixed azimuths. The results of the azimuthal dependence of the power, $Z_{DR\,(m)}$, and φ_{dp} are in Fig. 13.1. The fluctuations of Z_{DR} are mainly in the limits of plus minus one quantization interval. The same is valid for the differential phase. The elevation dependence of the parameters is presented in Fig. 13.2. One can see not significant variations of Z_{DR} and the differential phase over elevation.

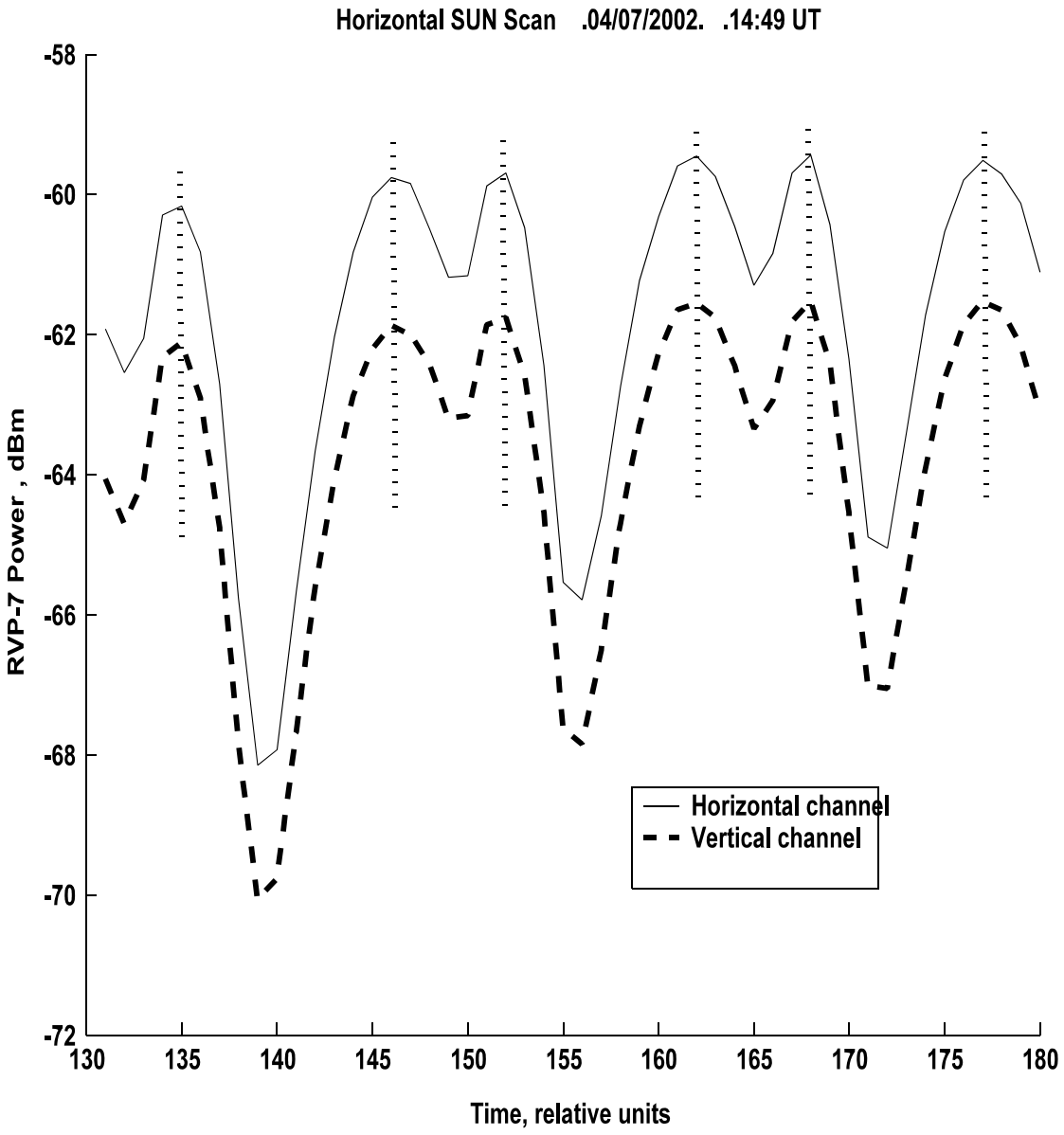

Fig. 12.1. Horizontal alignment of the H and V beams.

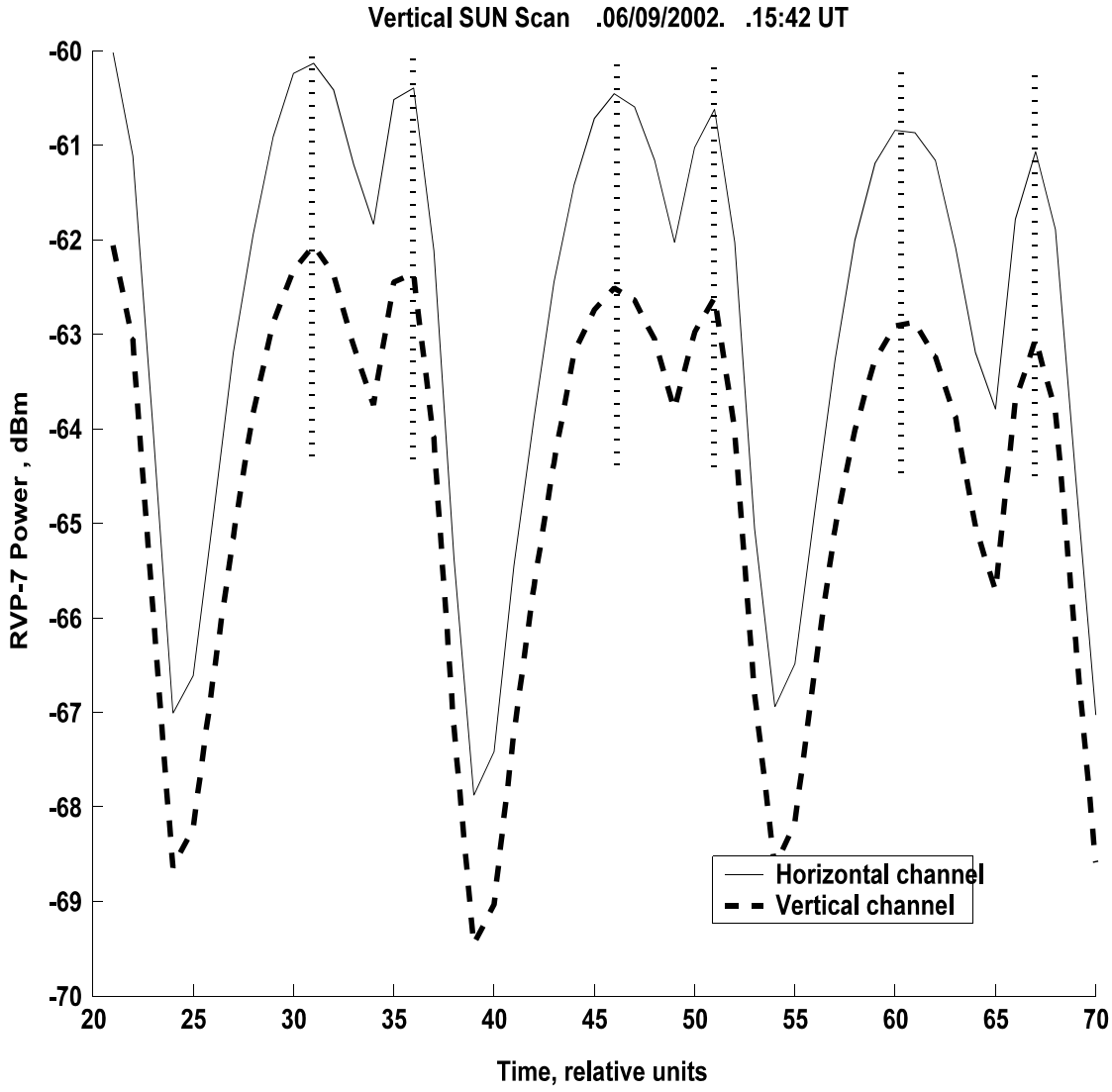

Fig. 12.2. Vertical alignment of the H and V beams

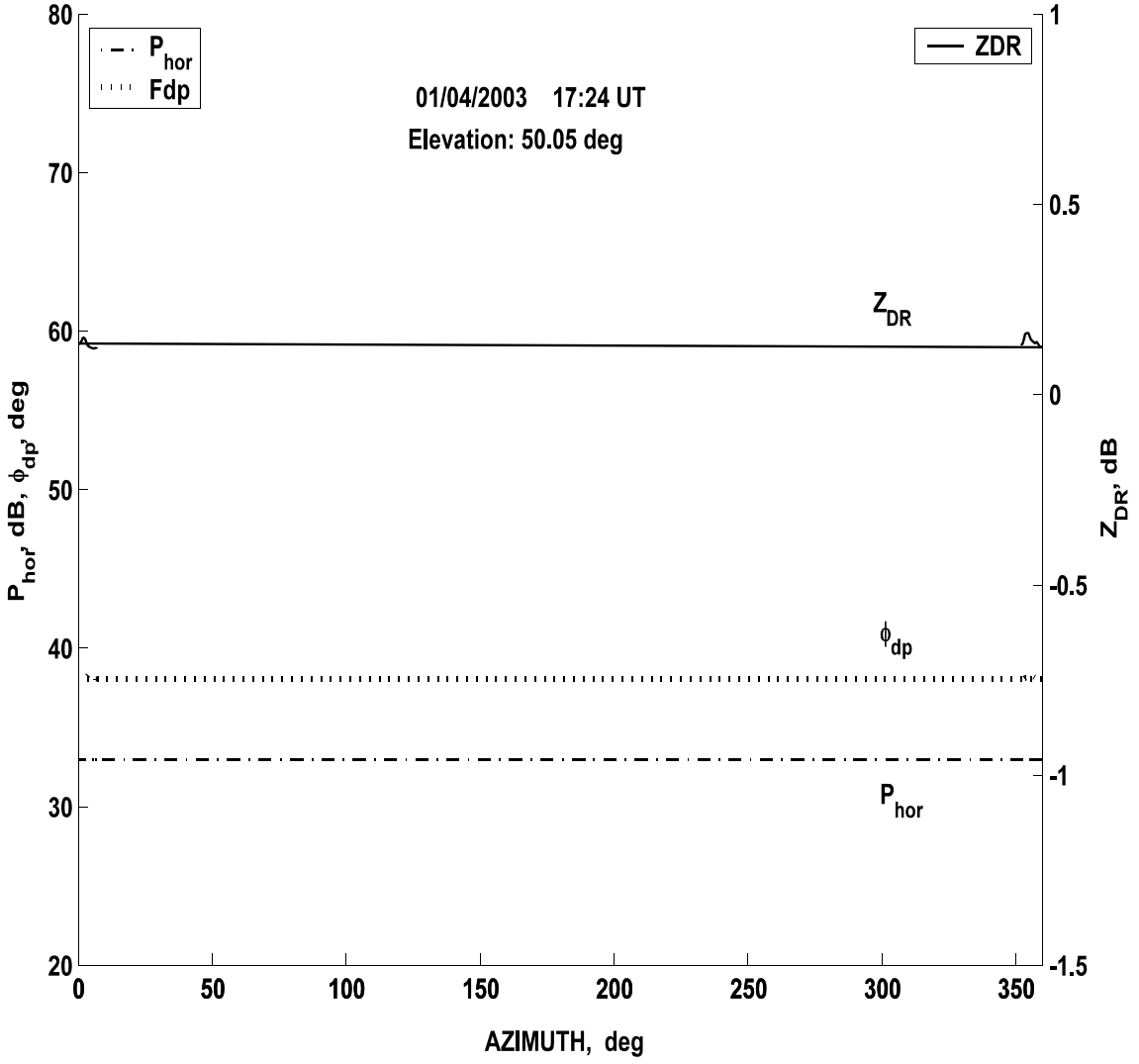

Fig. 13.1. Azimuthal dependence of the power in horizontal channel, P_{hor}, differential reflectivity, Z_{DR}, and differential phase φ_{dp}.

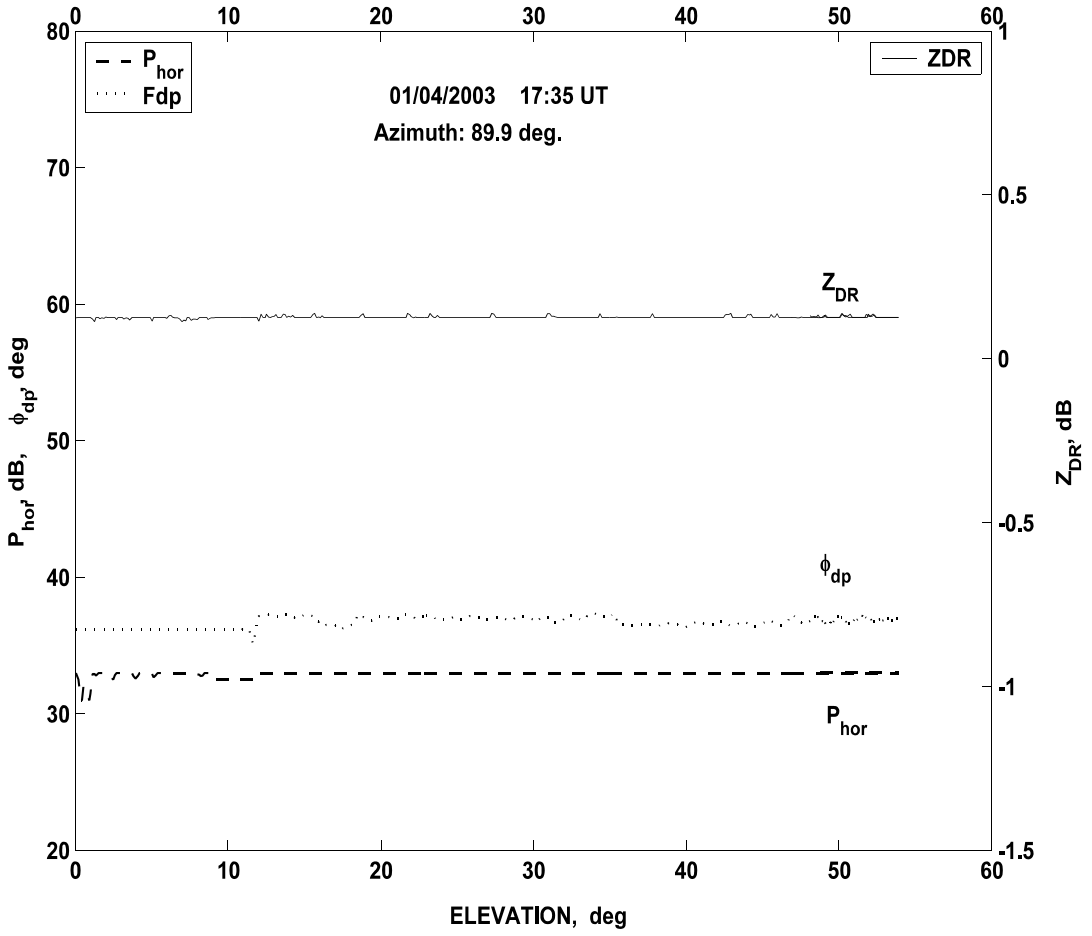

Fig. 13.2. Elevation dependence of the power in horizontal channel, P_{hor}, differential reflectivity, Z_{DR}, and differential phase φ_{dp}.

14. Summary

The NOAA's research WSR-88D with polarization capabilities has high isolation between polarization channels. In the Simultaneous transmission and reception of the Horizontally and Vertically polarized waves, SHV, the radar delivers the base radar moments, i.e., reflectivity, Doppler velocity, and spectral width, and three additional polarimetric variables: differential reflectivity, differential phase, and correlation coefficient between copolar signals. An example of these six fields is presented in Fig. 14.1 in a form of a vertical cross section.

In the SHV mode, two radar beams with H and V polarized waves are matched in boreside and beamwidths therefore the correlation coefficient is very high in rain. High values of the ρ_{hv}, (0.995) in light rain proves good polarization purity of the radar.

To calibrate the differential reflectivity, we employed several methods: we used the test signals from built-in radar generators, the sun scans, weather signals and ground clutter histograms. The system differential reflectivity $Z_{DR\ SYS}$ obtained with different methods are as follows:

Method	$Z_{DR\ SYS}$**, dB**	
Test signals	- 0.48	(Section 5.1)
Sun scans	- 0.38	(Section 5.2)
Weather signals	- 0.25	(Section 5.3)
Ground clutter	0	(Section 5.4)

Radar system differential reflectivity constants obtained with the first three methods are within about 0.2 dB. These measurements are stable and could serve as guideline for automatic calibration. Use of ground clutter histograms for calibrating the offset in differential reflectivity requires further evaluation. We recommend calibration of ZDR over the full dynamic range. In the present configuration with the RVP7 and offset IF this was cumbersome. Thus the procedure will be reevaluated when the RVP8 is installed. That processor will accept the same IF for horizontal and vertical channel and therefore the match between the bandwidths in these two channels will be much better. System differential phase is also very stable and exhibits relatively small fluctuations.

Overall the upgraded WSR-88D routinely produces polarimetric variables of exceptional quality. Engineering evaluation of the proof of concept is beyond our expectations and we are ready to commence development of a prototype for the WSR-88D network.

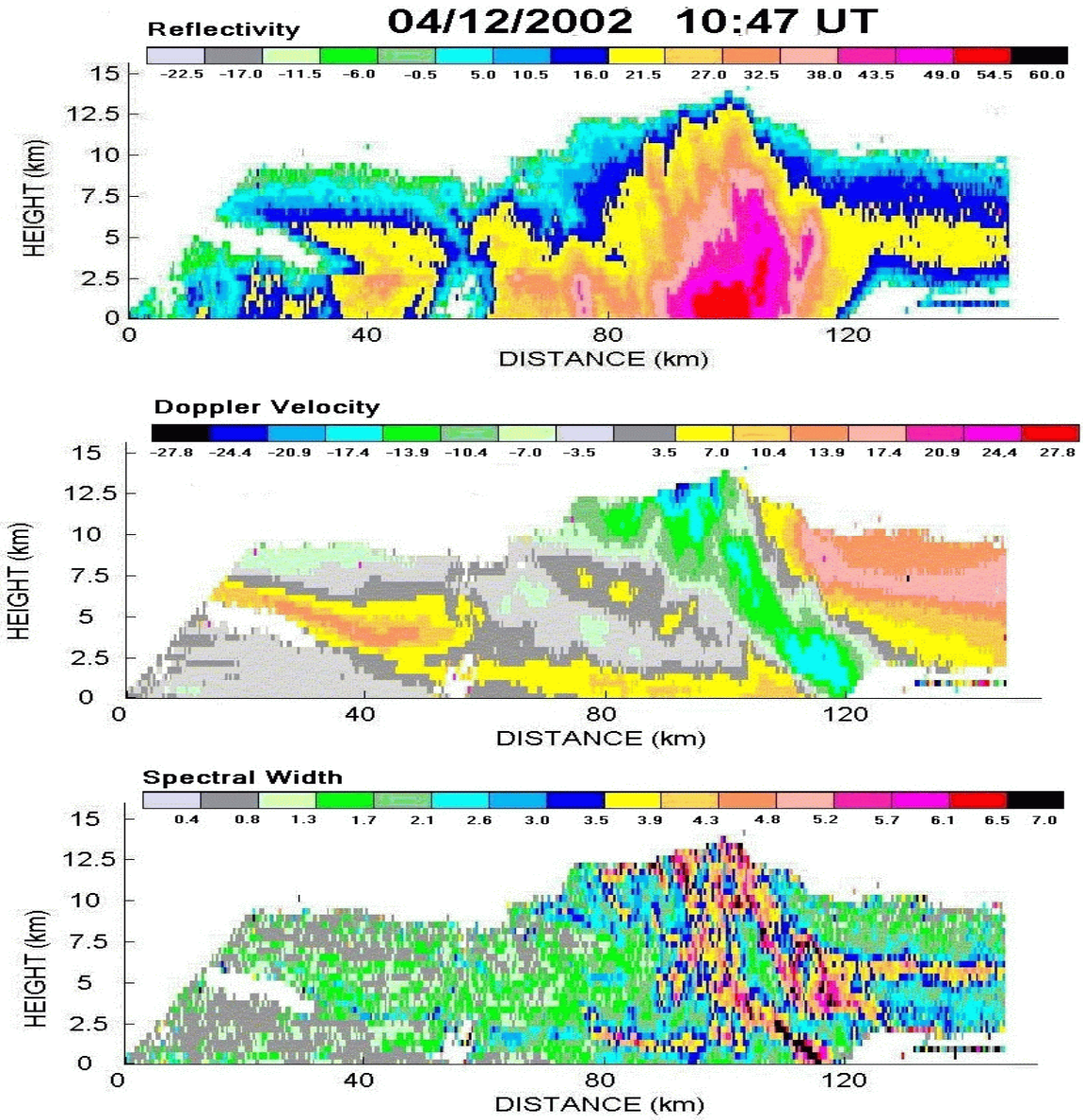

Fig. 14.1.a. Vertical cross-sections of the spectral moments: reflectivity, Doppler velocity, and spectral width.

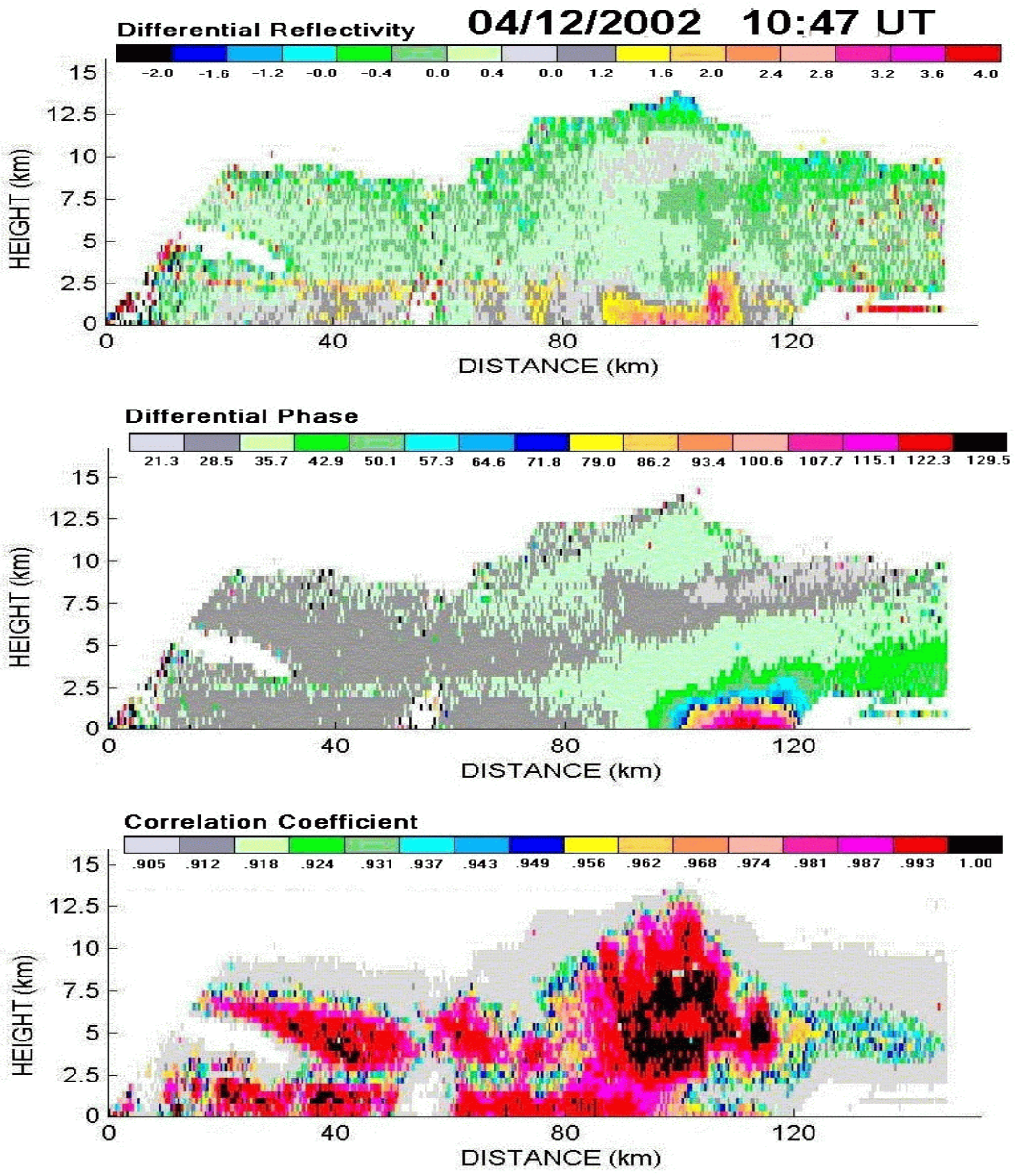

Fig. 14.1.b. Vertical cross-sections of fields of polarimetric variables: differential reflectivity, Differential phase, and correlation coefficient. SHV mode.

References

Atlas, D. 2002. Radar calibration. Some simple approaches. Bull. Amer. Met. Soc., v. 83, p. 1313- 1316.

Bringi, V. N. and V. Chandrasekhar, 2001: *Polarimetric Doppler Weather Radar. Principles and Applications.* Cambridge University Press. 636 pp.

Brunkow D., V. N. Bringi, P. C. Kennedy, S. A. Rutledge, V. Chandrasekar, E. A. Mueller, R. K. Bowie. 2000: A description of the CSU—CHILL national radar facility. J. Atmos. Ocean. Technol., **12,** 1596 - 1608.

Crum, T.D., R. L. Alberty, and D. W. Burgess, 1993: Recording, archiving, and using WSR-88D data. *Bull. Amer. Meteorol. Soc.*, **74**, 645 – 653.

Doviak, R. J. and D. S. Zrnic, 1993: *Doppler radar and weather observations*, 2nd ed., Academic Press, 562 pp.

Doviak, R. J., D. S. Zrnic, J. Carter, A. Ryzhkov, S. Torres, and A. Zahrai, 1998: Polarimetric upgrades to improve rainfall measurements. Report of the National Severe Storms Laboratory, Norman, OK 73069, 110 pp.

Doviak, R.J., V. N. Bringi, A. Ryzhkov, A. Zahrai, D. Zrnic, 2000: Considerations for polarimetric upgrades to operational WSR-88D radars. J. Atmos. Ocean. Technol., 17, 257 - 278.

Doviak, R. J., J. Carter, V. Melnikov, D. S. Zrnic. 2002. Modifications to the research WSR-88D to obtain polarimetric data. NSSL interim report.49 pp.

Melnikov, V., D.S. Zrnic, R. J. Doviak, J. K. Carter, 2002: Status of the dual polarization upgrade on the NOAA research and development WSR-88D. 18-th Internat. Conf. IIPS. Boston, AMS, p. 124 - 126.

Pratte, J. F., D. G. Ferraro. 1989: Automated solar gain calibration. 24-th Conf. Radar Meteorol. AMS, Boston, 619 -622.

Pratte, F., D. Ferraro. 1995. Improved WSR-88D Sun-source calibration Software and Procedures. Final Engineering Report. NWS/OSF. 85 pp.

Ryzhkov, A.**,** and D. Zrnic, 1998a: Discrimination between rain and snow with a polarimetric radar. *Journal of Applied Meteorology*, **37**, 1228-1240.

Ryzhkov, A., D. Zrnic and B. Gordon, 1998b: Polarimetric method for ice water content determination. *Journal of Applied Meteorology,* **37**, 125-134.

SIGMET, 2002: RVP7 Doppler Signal Processor; User's Manual. July. A technical document of SIGMET, Inc., Westford, MA USA.

Zrnic, D. S., 2001: Receiver - signal processor; distinction and implications for calibration; a paper presented to the AMS Radar Calibration workshop, Jan. 15, 2001, Phoenix, AZ.

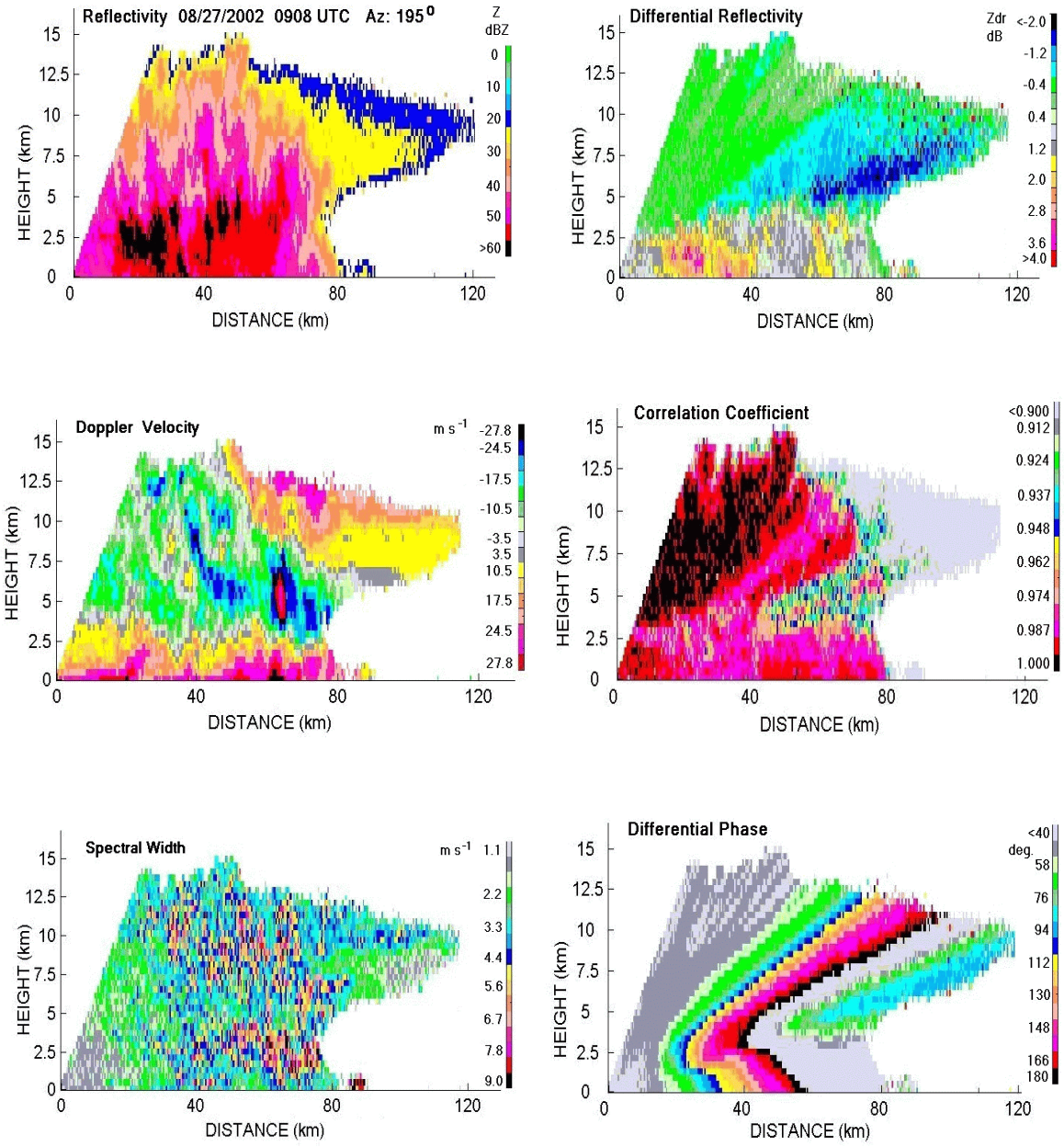

Vertical cross section of thunderstorm on Aug. 27, 2002 at 0908 UTC at azimuth of 195^0 recorded with the NSSL's WSR-88D in the SHV mode. The four fields from this set are in the front page of this report.